applied sciences

MDPI

Article

A Case Study on the Validation of Renewable Energy Grid Code Compliance for a Large-Scale Wind Power Plant Grid-Connected Mode of Operation in Real-Time Simulation

Sinawo Nomandela *, Mkhululi E. S. Mnguni and Atanda K. Raji

Department of Electrical, Electronic and Computer Engineering, Cape Peninsula University of Technology, Bellville, P.O. Box 1906, Cape Town 7353, South Africa; mngunim@cput.ac.za (M.E.S.M.); rajia@cput.ac.za (A.K.R.)
* Correspondence: snomandela@wsu.ac.za

Abstract: In this study, the grid-connected mode of operation was evaluated, considering the renewable energy grid codes. First, the renewable energy grid code specifications have been revisited, focusing mainly on large-scale renewable power plants. An interconnected system has been developed by combining the traditional electrical power grid with a large-scale wind power plant. The modeling method used in this study and how the evaluation has been conducted can be used for other power system evaluation studies. The results obtained from the interconnected system show a significant improvement in substation (or busbar) voltages.

Keywords: large-scale wind power plant (LSWPP); grid-connected mode of operation; renewable energy grid code (REGC); wind turbine generator unit (WTGU); voltage stability; wind power plant (WPP) integration

check for updates

Academic Editor: Alessandro Lo Schiavo

Received: 18 March 2025
Revised: 18 April 2025
Accepted: 13 May 2025
Published: 15 May 2025

Citation: Nomandela, S.; Mnguni, M.E.S.; Raji, A.K. A Case Study on the Validation of Renewable Energy Grid Code Compliance for a Large-Scale Wind Power Plant Grid-Connected Mode of Operation in Real-Time Simulation. *Appl. Sci.* **2025**, *15*, 5521. https://doi.org/10.3390/app15105521

Copyright: © 2025 by the authors. Licensee MDPI, Basel, Switzerland. This article is an open access article distributed under the terms and conditions of the Creative Commons Attribution (CC BY) license (https://creativecommons.org/licenses/by/4.0/).

1. Introduction

Wind power plants (WPPs) have continuously evolved globally and have become a significant participant in enhancing grid operation in most countries, showcasing the immense potential of renewable energy sources [1–8]. WPPs can be operated in one of two modes: standalone or grid-connected. In grid-connected mode, they provide extra power when the demand for loads in the power grid increases. In standalone mode, they act as an emergency supply for individual loads during power system outages [9,10].

WPPs are classified as small-scale or large-scale, depending on the size of the wind turbine generator units (WTGUs) they comprise. The size of these WTGUs is based on the rotor diameter (in meters), swept area (in square meters), and the standard power (in kilowatts) produced by the WTGU. Table 1 shows the lists of different sizes of WTGUs [11].

Large-scale wind power plants (LSWPPs) comprise large commercial wind turbine generator units (LCWTGUs).

On the other hand, WTGUs are classified into two by the axis at which wind turbine blades (WTs) rotate. They are horizontal-axis wind turbine generator units (HAWTGUs) and vertical-axis wind turbine generator units (VAWTGUs). HAWTGUs are the most popular class and are either upwind or downwind. Figures 1 and 2 show the upwind and downwind HAWTGUs [12]. Upwind HAWTGUs are the most popular class and are applied mostly in large-scale wind power plants (LSWPPs).

Table 1. Horizontal-axis wind turbine generator unit classification based on rotor diameter, swept area, and power rating.

		Rotor Diameter (m)	Swept Area (Square Meters)	Standard Power Rating (Kilowatts)
Small-scale	Micro	0.5–1.25	0.2–1.2	0.004–0.25
	Mini	1.25–3	1.2–7.1	0.25–1.4
	Household	3–10	7–79	1.4–16
Small commercial		10–20	79–314	25–100
Medium commercial		20–50	314–1963	100–1000
Large commercial		50–100	1963–7854	1000–3000

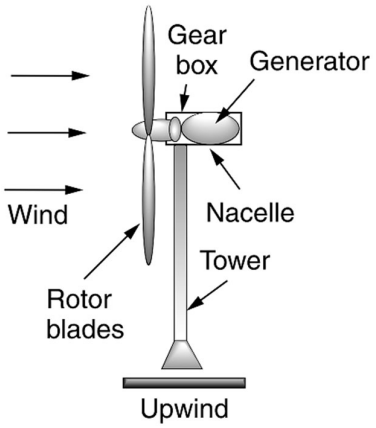


Figure 1. Upwind horizontal-axis wind turbine generator unit [12].

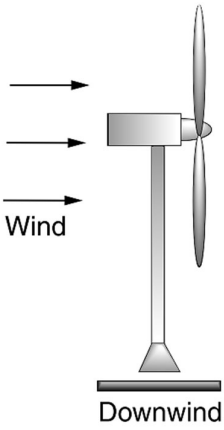


Figure 2. Downwind horizontal-axis wind turbine generator unit [12].

The operation of LSWPPs in a grid-connected mode has been leading over the past ten years [13–15]. Many studies have been conducted regarding LSWPPs in grid-connected modes of operation. However, few studies have examined the renewable energy grid code (REGC) specifications while integrating these LSWPPs into the power grid. Among the few, none have evaluated various operating conditions of the power grid into which the LSWPP is (or is to be) integrated.

For instance, a study in [16] conducted an assessment of the grid-connected mode of operation for an offshore LSWPP. The study compared the cost margin when the power transmission from an offshore LSWPP is alternating current (AC) or direct current (DC). The study aimed to prove little significance in choosing DC over AC when transmitting power

from an offshore LSWPP to the power grid. However, it did not consider ensuring the LSWPP meets the grid code specifications before integration. This oversight underscores the crucial role of REGC in the operation of LSWPPs.

A study of integrating a LSWPP into a weak distribution network was conducted in [17]. A 6 MW single WTGU that was sufficiently sized to approximate the acceptable megawatt capacity of a WPP was used in the study. Additionally modeled in this study was a 9 MW single WTGU for grid integration using the static synchronous compensator (STATCOM) [18]. The impact integration of wind power plants (WPPs) and wind turbine generator units (WTGUs) has on power system stability has been studied in the references [19–21]. None of these models were initially performed independently for grid compliance tests as required by the REGCs.

Considering the models used in [17–21], it is understood that the computation of each component consumes time. However, these models may not provide adequate validation to align the REGCs. This violates the design and operational requirements of WPPs mentioned in [22–24].

An interconnected system was developed by integrating a LSWPP with the IEEE 9 Bus Power System in [25]. The study mainly focused on developing the point of common coupling (PCC) protection system that adapts to the conditions of the interconnected system and responds to the faulty conditions for both normal and increased loading conditions.

The work published in references [1,3,4,14,26] emphasized the significance of REGCs for LSWPPs in the grid-connected mode of operation.

The significant gap in all the studies reviewed above is that none have studied the LSWPP alone to ensure its operation meets the REGC specifications before integrating it into the considered power grid. This work stands out in the field due to its unique approach of combining REGC discussions with case studies. This approach provides a better understanding of the implications of integrating large-scale WPPs into the power grid. The significance of this work lies in its focus on the REGCs requirements, a crucial yet underexplored subject in the realm of renewable energy. Our revisit to these requirements, with the evaluation performed using a case study, promises to shed new light on their role in integrating LSWPPs, underscoring their importance in the field.

Following the introduction of this article, Section 2 revisits REGCs with an emphasis on WPPs. The overview of the proposed test system is in Section 3. This includes the modeling and simulation consisting of a few case studies of the power grid into which the LSWPP is integrated and the LSWPP itself. In contrast, the integration of the LSWPP into the power grid is dealt with in Section 4. Section 5 is dedicated to the crucial evaluation of the operation of the interconnected system, which also formulates an essential aspect of our research. Section 6 discusses the results. Finally, conclusions and future work are drawn and stated in Section 7.

2. Overview of Renewable Energy Grid Code Specifications

The REGCs are a set of technical standards and requirements to be followed when connecting renewable energy sources to the power grid [10,23,24].

Since the voltage level at which the RPPs are integrated into the power grid is significant, we first recap the standard voltage levels. We will then categorize the RPPs at a later stage. It should be noted that standard voltage levels differ depending on the country. For example, one of the Asian articles that categorized the voltage levels at which various WPP categories are integrated also provided some information on the Saudi Arabian standard voltages. This information is presented in Table 2 [1].

Table 2. Saudi Arabian standard grid voltages at which various types of wind power plants are integrated.

Category		Wind Power Plant Group	Voltage (kV)
Transmission	Normal transmission	Offshore: Group 1 or Group 2	400
			220
			132
	Sub-transmission	Onshore	66
Distribution		Small wind turbines	33
			11

However, this article defines voltage levels based on the South African power grid. The National Energy Regulator of South Africa (NERSA) [24] and ESKOM [27] categorizes the grid standard voltage as shown in Table 3.

Table 3. South African standard grid voltages.

Category		Voltage (kV)	Level
Transmission	Normal transmission	765	Extra-high
		400	
		275	
	Sub-transmission	132	High
Distribution		66	
		50	
		33	Medium
		25	
		22	
		11	

RPPs are categorized into three, based on their minimum and maximum apparent power production and the voltage level at which they can be integrated into the power grid. The first category is A (with subcategories A1, A2, and A3), followed by B and C. Table 4 lists the RPP categories and specifies the voltage levels at which the RPP category can be integrated [23].

Table 4. South African renewable power plant categories.

Category		Minimum Capacity (kVA)	Maximum Capacity (kVA)	Integration Level Voltage
A	A1	0	13.8000	LV
	A2	13.8000	100	LV
	A3	100	1000	LV
B		0	20,000	MV
C		>20,000	-	MV/HV

WPPs made of squirrel-cage induction generators (SCIGs) may have reactive power support in the power grid since their stator terminals are coupled with capacitor bank exciting circuits. However, this reactive power is minimal [1].

The work presented in this article mainly focuses on WPPs, whilst the discussions regarding renewable energy grid codes (REGCs) are based entirely on RPPS. Therefore, in this article, for discussions on REGCs, the term RPP instead of WPP is used.

2.1. Tolerance of Frequency and Voltage Deviations

2.1.1. Normal Operating Conditions

RPPs must be designed to operate continuously within the point of common coupling (PCC) voltage range specified in Table 5 [24,28], measured at the PCC.

Table 5. Minimum and maximum operating voltages at the point of common coupling.

Nominal Voltage (V_N) in Kilovolt	Minimum V_N (PU)	Maximum V_N (PU)
132.0000	0.9000	1.0985
88.0000	0.9000	1.0985
66.0000	0.9000	1.0985
44.0000	0.9000	1.0800
33.0000	0.9000	1.0800
22.0000	0.9000	1.0800
11.0000	0.9000	1.0800

RPPs must be designed to operate within the minimum range illustrated in Figure 3 during a system frequency disturbance. It must be disconnected from the power grid should it experience a frequency higher than 51.5000 Hz for longer than 4 s or a frequency lower than 47.0000 Hz for longer than 200 ms. Also, the RPPs must remain connected to the power grid when they experience a rate of frequency change with values of 1.5000 Hz per second as long its minimum frequency is still within the minimum and maximum frequencies of 49.0000 HZ and 51.0000 Hz [24,28].

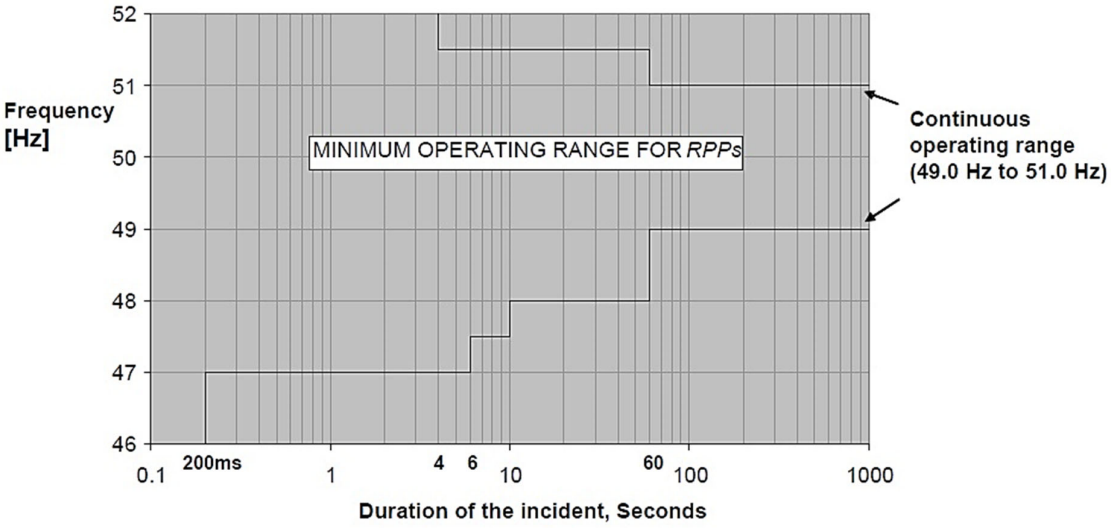


Figure 3. Minimum frequency operating range of renewable power plants during system frequency disturbances [24,28].

RPPs must only be connected to the power grid as early as 3 s after the following conditions have been met [24,28]:

- For transmission level-connected RPPs, the voltage at the PCC is within +/−5% of the nominal voltage.
- For distribution level-connected RPPs, the PCC voltage is within the minimum and maximum V_N specified in Table 5.
- Frequency in the RPP is within 49.0000 Hz and 50.2000 Hz or otherwise stated as agreed with the system operator (SO).

2.1.2. Abnormal Operating Conditions

RPPs must be built to tolerate abrupt phase changes of 20 degrees at the PCC without disconnecting or lowering its output. They must return to normal production within 5 s of the operating parameters of the PCC returning to normal following the settling time. They must also be designed to withstand and fulfill the PCC voltage conditions described in Table 5 and Figure 4. Area D in the figure is mainly for Category C RPPs. Furthermore, RPPs must withstand PCC voltage drops for a minimum duration of 0.150 s without disconnecting, as shown in Figure 4 [24,28].

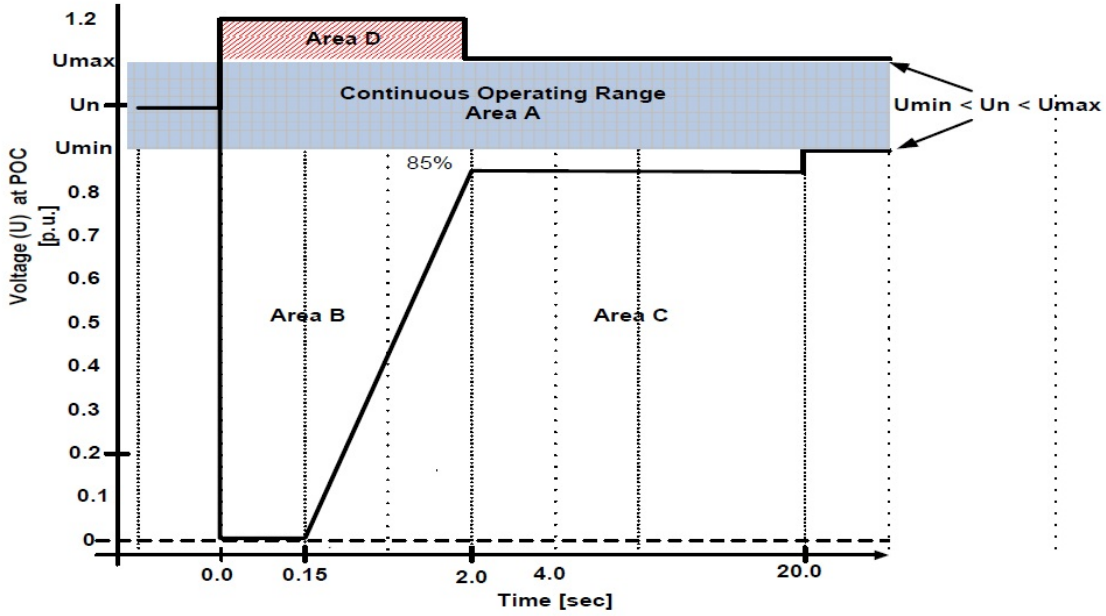


Figure 4. Voltage ride-through capability for renewable power plants of Category A3, B, and C [24,28].

RPPs must be designed to withstand voltage droops and peaks, as illustrated in Figure 5 [24,28]. As the figure illustrates, it must supply or absorb reactive current without disconnecting.

2.2. Frequency Response

RPPs must be built to offer a power–frequency response to stabilize the power grid frequency in the event of frequency deviations. RPPs must be able to meet the required active power reduction needs to stabilize the frequency during high-frequency operating situations (see Figure 6) [24,28].

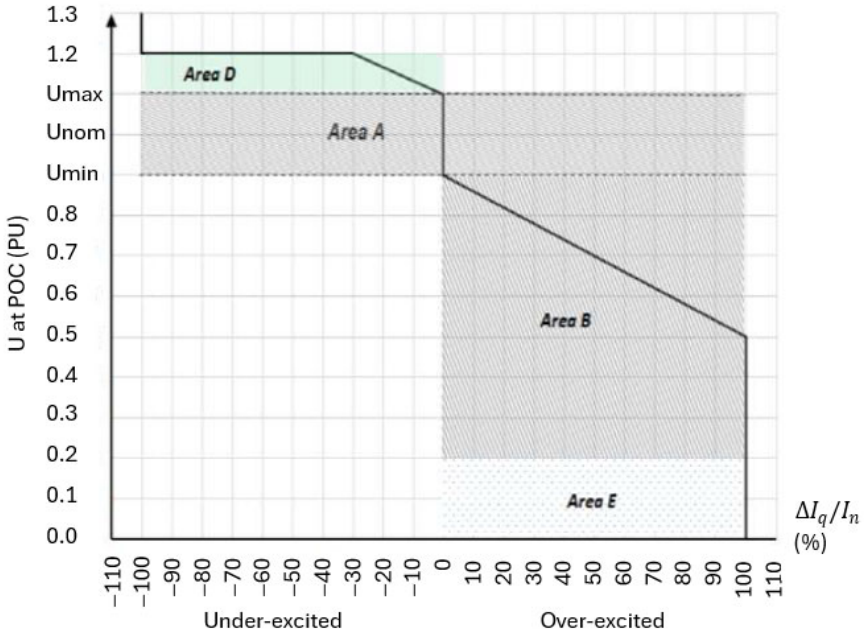


Figure 5. Requirements for reactive power support during the voltage drops and peaks at the point of common coupling [24,28].

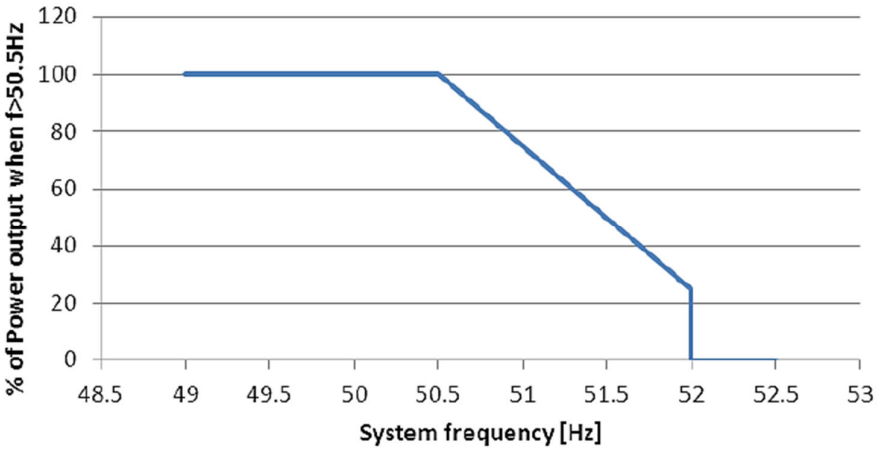


Figure 6. Power curtailment during over-frequency for renewable power plants [24,28].

The accuracy of grid frequency measuring must be at least +/−10 mHz. When the power grid frequency increases above 50.5000 Hz, RPPs must reduce the active power proportionate to the frequency change, as illustrated in Figure 6. RPPs must be disconnected if the frequency exceeds 51.5000 Hz for more than four seconds to protect the electrical grid [24,28].

2.3. Reactive Power Capabilities for Category C

RPPs must be designed to operate in one of three control modes: power factor, voltage, or reactive power (Q or Mvar). It is necessary to agree on the control operating mode (Q, power factor, or V control) and the network service provider (NSP). When operating between 5% and 100% of rated power Pn (MW), the RPPs must be able to adjust reactive power (Mvar) support at the PCC within the reactive power capacity ranges depicted in Figure 7, where Qmin and Qmax are voltage-dependent, as seen in Figure 8 [24,28].

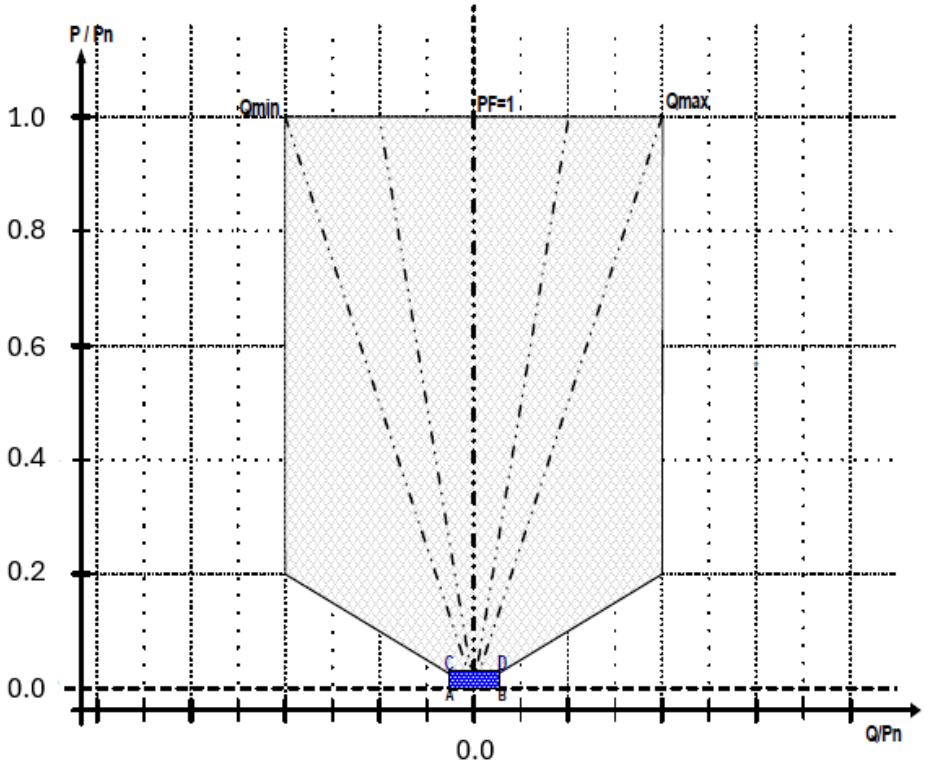


Figure 7. Reactive power requirements for renewable power plants of Category C at the point of common coupling (Qmin and Qmax are voltage-dependent, as defined in Figure 8) [24,28].

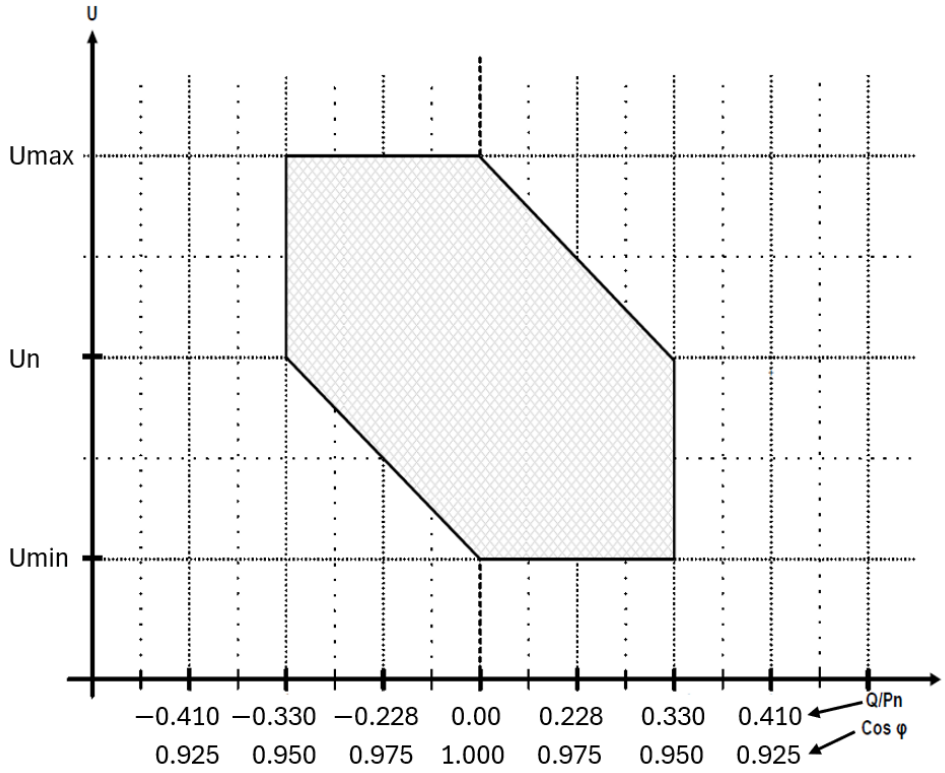


Figure 8. Requirements for reactive power and voltage control range for renewable power plants of Category C [24,28].

Figure 9 shows the necessary RPP reactive power capability (determined at the PCC) at nominal voltage. No reactive power capability is needed when operating at less than 5% of the rated power Pn (MW). As Figure 9 illustrates, the RPP can only function within

the reactive power tolerance range not over +/−5% of rated power in Areas A, B, C, and D [24,28].

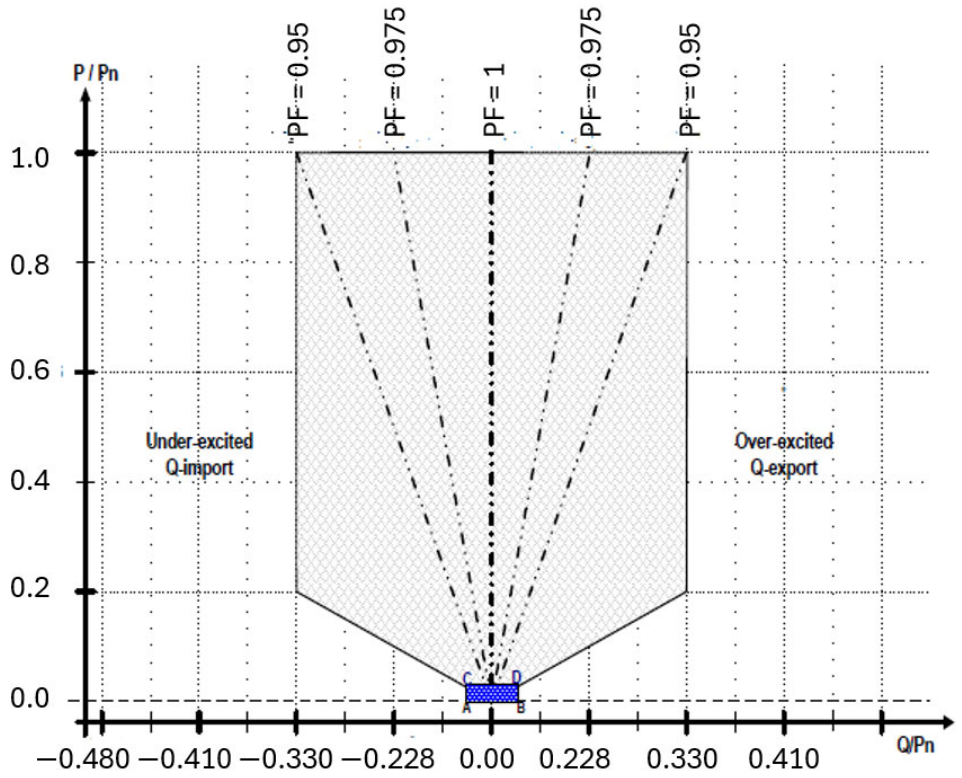


Figure 9. Reactive power requirements for renewable power plants of Category C (at the nominal voltage at the point of common coupling) [24,28].

2.4. Voltage and Reactive Power Control Functions

Reactive power control functions that can regulate the reactive power that the RPP supplies at the PCC and a voltage control function that can regulate the voltage at the PCC through commands utilizing setpoints and gradients are required for RPPs. Reactive power and voltage control are mutually incompatible, so the three functions, voltage control, power factor control, and reactive power control, can only be engaged simultaneously [24,28]. Moreover, the RPP generator will be employed to carry out the control function and apply parameter settings for reactive power and voltage control functions, which the NSP will decide in coordination with the SO. The operational agreement must include documentation of the agreed-upon control functions [24,28].

Reactive power control

Regardless of the active power and voltage, Q control regulates the reactive power supply and absorption at the PCC. Figure 10 shows this control function as a vertical line. The RPP generator must respond to any changes made to the Q control setpoint by the NSP, SO, or their agent within two seconds by updating its echo analog setpoint value. When an instruction to modify the setpoint is received, the RPP must react to the new setpoint within 30 s. The setpoint and the accuracy of the control must not differ by more than ±2% of the setpoint value or by ±0.5% of the maximum reactive power, whichever produces the highest tolerance. The RPP must receive a Q setpoint with a minimum precision of 1 kVAr [24,28].

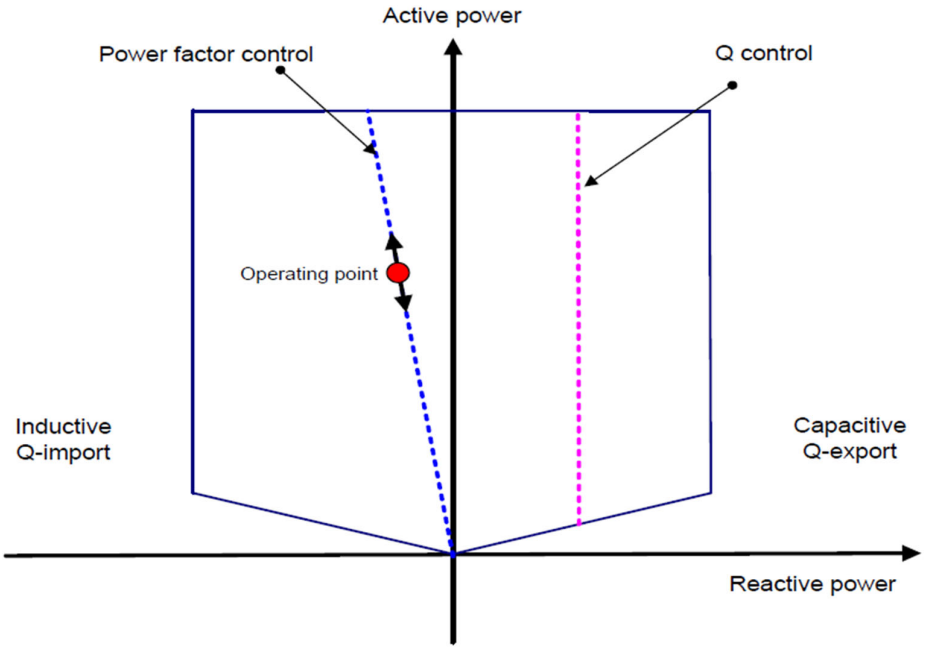


Figure 10. Reactive power control functions for a renewable power plant [24,28].

Power factor control

The power factor control function regulates reactive power at the PCC proportionately to active power. An example is a line with a constant gradient in Figure 10. If the NSP, SO, or their agent modifies the power factor setpoint, the RPP has to update its echo analog setpoint value within 2 s. When a command to change the setpoint is received, the RPP has 30 s to respond with the updated setpoint. The maximum difference between the control accuracy and the setpoint is ±0.02 [24,28].

Voltage control

One feature that regulates the voltage at the PCC is voltage control. If a modification is to be made to the voltage setpoint, it must start within 2 s and be finished within 30 s after receiving the command. Droop characteristics, as seen in Figure 11, require that the accuracy of the voltage setpoint be within ±0.5% of the nominal voltage and that the precision of the control be within ±2% of the required injection or absorption of reactive power [24,28].

With the droop setup as in Figure 11, each RPP can regulate within its dynamic range and voltage limit. Droop is defined here as the change in voltage (per unit) brought on by a change in reactive power (per unit). The control function will wait for potential overall control from the tap changer or other voltage control functions once the voltage control has reached the dynamic design limits of the RPP. Together with the SO, the NSP will be in charge of total voltage coordination [24,28].

2.5. Comparison with International Grid Codes

This study focused primarily on the renewable energy grid code (REGC) specifications of South Africa (SA), as regulated by the National Energy Regulator of South Africa (NERSA) and Electrical Supply Commission (ESKOM). Recognizing that REGCs for renewable power plant (RPP) integration vary across different electrical power systems worldwide is significant. Nonetheless, most international REGCs share fundamental operational requirements concerning continuous operating voltage and frequency ranges, active power control capabilities, reactive power support and control functions, fault ride-through (FRT) capabilities, frequency response, and stability requirements. For instance, the German

BDEW Medium Voltage Directive, the UK National Grid Code, and the IEEE 1547 Standard for Interconnection of Distributed Energy Resources in the USA set comparable technical requirements for voltage and frequency tolerance, reactive power capability, and grid fault behavior [29–31].

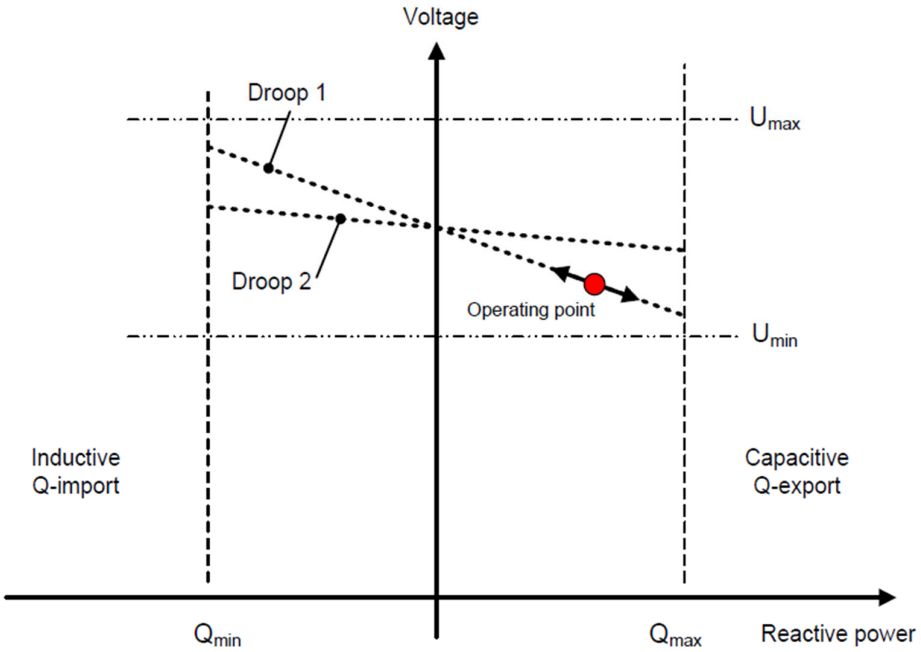


Figure 11. Voltage control of a renewable power plant [24,28].

However, differences typically arise in specific voltage ride-through curves, the permissible ranges of power factor adjustment, the exact frequency thresholds and response times, and the operational control modes, such as voltage versus power factor versus reactive power control priority.

The LSWPP model developed in this study was validated against REGCs of SA, which serve as a representative framework for Category C LSWPP. Given the similarity in core requirements across most international standards, the model can be adapted for other regions by adjusting the reactive power control ranges and setpoints, modifying the acceptable frequency and voltage operation limits, tuning the FRT capability curves and thresholds according to the REGCs of the target region.

This adaptability is possible because the model was built using flexible, parameterized control components within the Real-time Simulation Computer-Aided Design (RSCAD) simulation environment. Therefore, while the present study validated compliance based on SA standards, the methodology and simulation framework remain applicable for evaluating LSWPPs against other regional grid codes with minor parameter adjustments.

3. Overview and Development of the Proposed Test System Considered for the Study

This study evaluated the grid-connected mode of operation of the large-scale wind power plant (LSWPP). Operating the LSWPP in a grid-connected mode forms the modern power grid. On the other hand, a modern power grid combines any renewable power plant (RPP) and the traditional electrical power grid.

This section describes the traditional electrical power grid and the LSWPP considered in this study.

3.1. The Power Grid System Considered for the Study

The IEEE 9 Bus Power System is used in this study due to its simplicity, well-documented data availability, and established use in renewable integration studies. There are other publications in which the system has been used. For instance, in reference [19], it was used for another study dealing with renewable power plant (RPP) integration. The IEEE 9 Bus Power System allows the performance of power grid case studies that significantly complement the need for a large-scale wind power plant (LSWPP) integration.

3.1.1. Preparation of the IEEE 9 Bus Power System

The model of the IEEE 9 Bus Power System is available in the Real-time Simulator Computer-Aided Design (RSCAD) software, version FX 1.3 instruction manual from RTDS Technologies Inc., referenced in [32]. Below is a significant recap of how the components were modified from the original IEEE 9 Bus Power System in the RSCAD software instruction manual.

The components were rearranged and renamed, as shown in Table 6. The modified system is shown in Figure 12.

Table 6. Renaming of components for the modified IEEE 9 Bus Power System.

Original Name		Modified Names	
Busbar	**Component Connected to It**	**Busbar**	**Component Connected to It**
1	G1	G1Bus	Gen1
2	G2	G2Bus	Gen2
3	G3	G3Bus	Gen3
4	None	Bus1	None
5	Unnamed load 1	Bus2	DLoad1
6	Unnamed load 2	Bus3	DLoad2
7	None	Bus4	None
8	Unnamed load 3	Bus5	DLoad3
9	None	Bus6	None

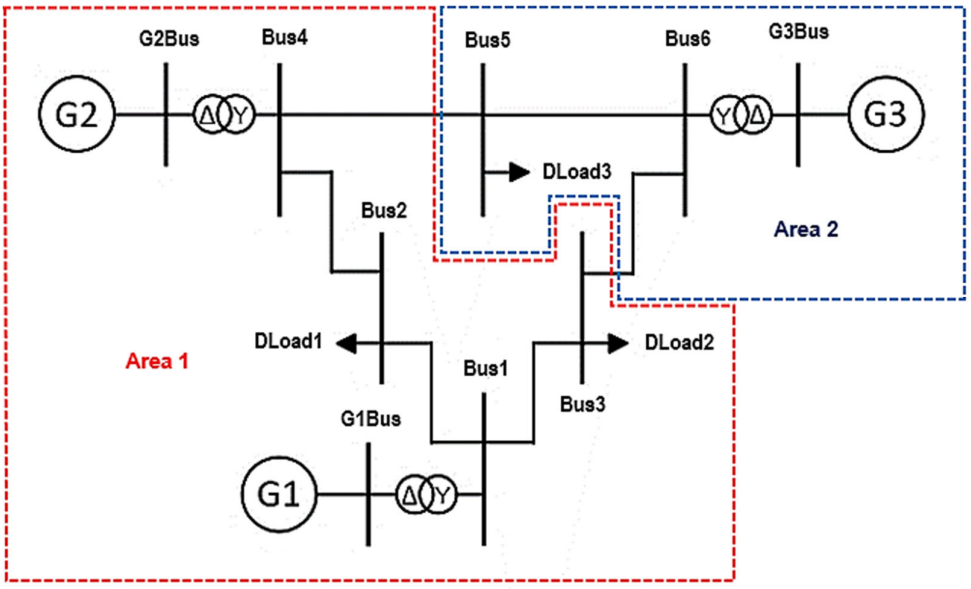


Figure 12. Modified IEEE 9 Bus Power System, adapted from the previous studies [32].

Area 1 and Area 2 in Figure 12 represent subsystems on RSCAD. These real-time simulations for an electrical system of two subsystems are performed in two RTDS hardware racks, Rack 1 and Rack 2. In the rest of this article, the two terms subsystems and racks are used interchangeably because they have the same meaning.

The transmission line parameters of the IEEE 9 Bus Power System have been listed in Table 7. All per unit values have been derived from a base apparent power of 100 MVA [32].

Table 7. IEEE 9 Bus Power System transmission line parameters.

Lines	Busbar to Which Line Is Connected	Length (km)	Resistance (PU)	Reactance (PU)	Susceptance (PU)
Line12	Bus1–Bus2	89.9300	0.0100	0.0850	0.1760
Line13	Bus1–Bus3	97.3360	0.0170	0.0920	0.1580
Line24	Bus2–Bus4	170.3380	0.0320	0.1610	0.3060
Line36	Bus3–Bus6	179.8600	0.0390	0.1700	0.3580
Line45	Bus4–Bus5	76.1760	0.0085	0.0720	0.1490
Line56	Bus5–Bus6	106.6460	0.0119	0.1008	0.2090

RSCAD consists of two modules, namely the draft and runtime modules. The draft module deals with the modeling of the system itself, while the runtime module deals with the real-time simulations of the modeled system. The modeling on the draft module deals with gathering components that make up a power system model. This includes control components, such as control switches, sliders, pushbuttons, and other operating systems.

After the completion of the model, the draft load flow simulation was executed to verify data accuracy and the initial conditions of the modeled system. Results were obtained and recorded in Table 8. These results are the same as those found in [32].

Table 8. Initial conditions of the IEEE 9 Bus Power System.

Bus	Bus Type	Voltage (PU)	P_G (MW)	Q_G (MVAr)	P_L (MW)	Q_L (MVAr)
G1Bus	Slack	1.0400∠0.0000°	71.7798	36.2675	-	-
G2Bus	PV	1.0250∠8.3639°	163.0000	11.2300	-	-
G3Bus	PV	1.0250∠4.0221°	85.0000	−3.7204	-	-
Bus1	PQ	1.0207∠27.7678°	-	-	-	-
Bus2	PQ	0.9928∠26.3247°	-	-	125.0000	50.0000
Bus3	PQ	1.0064∠26.5655°	-	-	90.0000	30.0000
Bus4	PQ	1.0230∠32.7884°	-	-	-	-
Bus5	PQ	1.0128∠30.2929°	-	-	100.0000	35.0000
Bus6	PQ	1.0283∠31.3133°	-	-	-	-

It has been stated in the references [33–35], that the reactive power transfer through substations (busbars) causes voltage stability challenges in the power grid. In this study, the assumption has been made that the increase in load demand means an increase in active and reactive power. We, therefore, configured the load increase simulation logic, as shown in Figure 13.

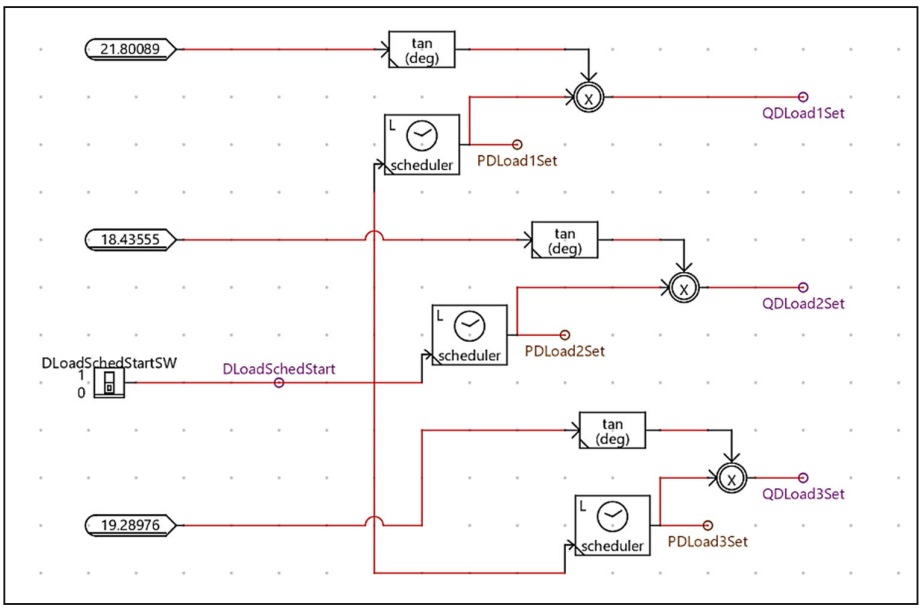


Figure 13. Logic for load schedular and direct proportionality of active and reactive power demand.

PDLoad1Set and *QDLoad1Set* in the figure are signal names to control the three loads, DLoad1, DLoad2, and DLoad3. *DLoadSchedStart* is a digital signal from a binary switch that controls the status (*ON*/*OFF*) of the scheduler component. The "scheduler" component multiplies the starting power levels by the specified multiplier to increase the load demand. The active power input signal of the dynamic loads is multiplied by the "tan (deg)" component. Reactive power to the load is shown by the output signal *QDload1Set*, which is based on the simultaneous rise in variables P and Q to maintain a constant load power factor. The power demand in the runtime module simulation platform will remain in its initial state until the switch DLoadSchedStartSW is turned on. The scheduler for each bulk load DLoad1, DLoad2, and DLoad3 is set to increase the load demand by 5.0000 MW every 0.1 s. An example is DLoad1, which has an initial active and reactive power of 125.0000 MW and 50.0000 MVAr. After 0.1 s, the load starts to draw 130.0000 MW and 51.9986 MVAr. And after 0.2 s, it starts to draw 135.0000 MW and 53.9986 MVAr.

To summarize the operation of the logic in Figure 13, the Expressions (1) to (3) are used.

Incremental increase in active power and reactive power:

$$P_{New} = P_{Old} + \Delta P \tag{1}$$

$\Delta P = 5$ MW every 0.1 s.

Reactive power is proportional to active power:

$$Q = P \times \tan(\varnothing) \tag{2}$$

The power factor $\cos(\varnothing)$ is calculated from the initial conditions. For example, for DLoad1 $P_0 = 125$ MW, $Q_0 = 50$ MVAr, then

$$\tan(\varnothing) = \frac{Q_0}{P_0} = 0.4$$

So,

$$Q_{New} = Q_{Old} + 0.4 \tag{3}$$

In real-world scenarios, this is when the loads connected to the electrical power grid increase. These simulations of load increase every 0.1 s. This simulation looks into what might happen regarding electrical power grid loading in the future.

3.1.2. IEEE 9 Bus Power System Simulations

Initial load demand simulations for the power grid

An initial load demand was simulated for the power grid. Tables 9 and 10 show the active and reactive power of the loads and busbars under initial load conditions, while Table 11 shows the voltages on the busbars Bus1, Bus2, Bus3, Bus4, Bus5, and Bus6.

Table 9. Active power on load busbars and their loads under initial load demand for the power grid.

	Load Active Power (MW)	Busbar Active Power (MW)
DLoad1 | Bus2	125.0000	125.0000
DLoad2 | Bus3	90.0000	90.0000
DLoad3 | Bua5	100.0000	100.0000

Table 10. Reactive power on load busbars and their loads under initial load demand for the power grid.

	Load Reactive Power (MVAr)	Busbar Reactive Power (MVAr)
DLoad1 | Bus2	50.0000	50.0000
DLoad2 | Bus3	30.0000	30.0000
DLoad3 | Bua5	35.0000	35.0000

Table 11. Busbar voltages under initial load demand for the power grid.

Busbars	Voltage (PU)
Bus1	1.0210
Bus2	0.9928
Bus3	1.0060
Bus4	1.0230
Bus5	1.0130
Bus6	1.0280

We used tables to present these results because the time parameter is insignificant since no disturbances were simulated.

Increased load demand simulations for the power grid

An increase in load demand was simulated to identify the voltage stability collapse point, which might be any voltage outside the range of 0.9500 and 1.0500 per unit based on power system grid codes. The voltages were observed in this simulation for busbars Bus1 to Bus6 in response to the load demand increase in different loads DLoad1, DLoad2, and DLoad3. It was identified that the voltage at Bus2, where DLoad1 is connected, could not recover and, therefore, is critical. This is because it settled and fell to 0.9486 per unit, out of the range of 0.9500 and 1.0500 per unit. This behavior is when the load demand of DLoad1 was raised by 5.0000 MW and 1.9999 MVAr every 0.1 s, which in total ended up in the value of 160.0000 MW and 65.0535 MVAr.

Figures 14–19 plot the active and reactive power demands of the loads DLoad1, DLoad2, and DLoad3 and the corresponding power at specific buses Bus2, Bus3, and Bus5. The voltage plots due to the active and reactive power demands of these loads are shown in Figures 20–25.

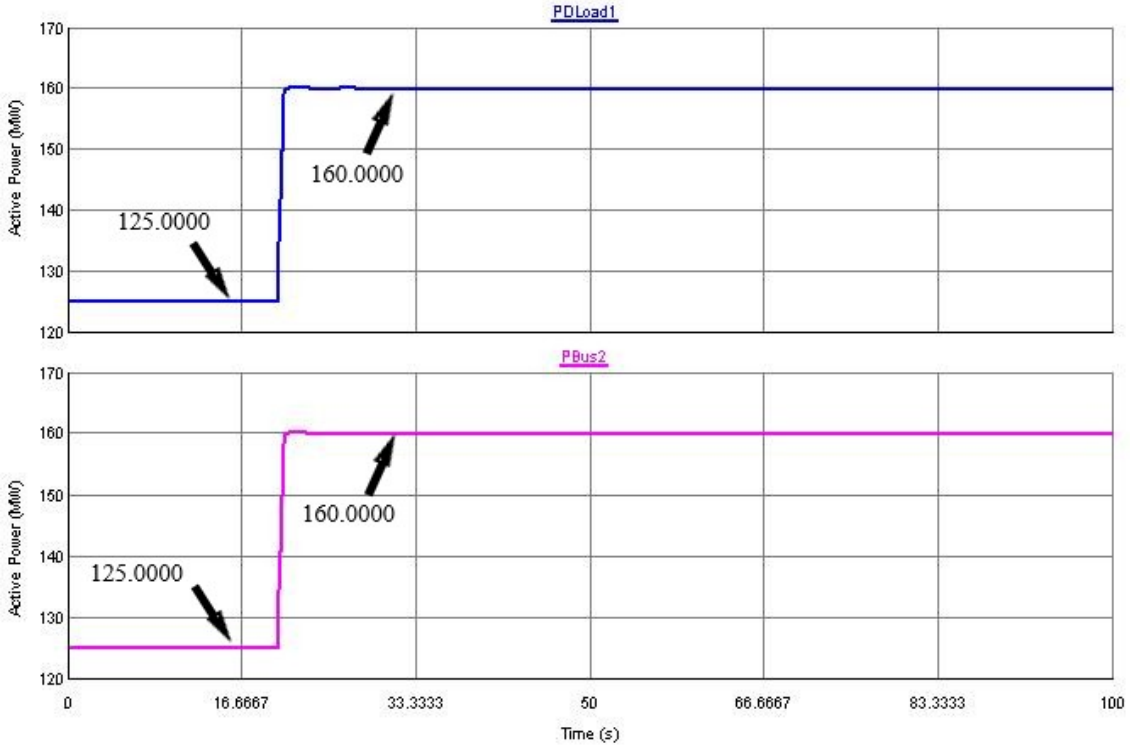


Figure 14. Increased load demand simulations for the power grid: Active power demand by DLoad1 and active power at Bus2.

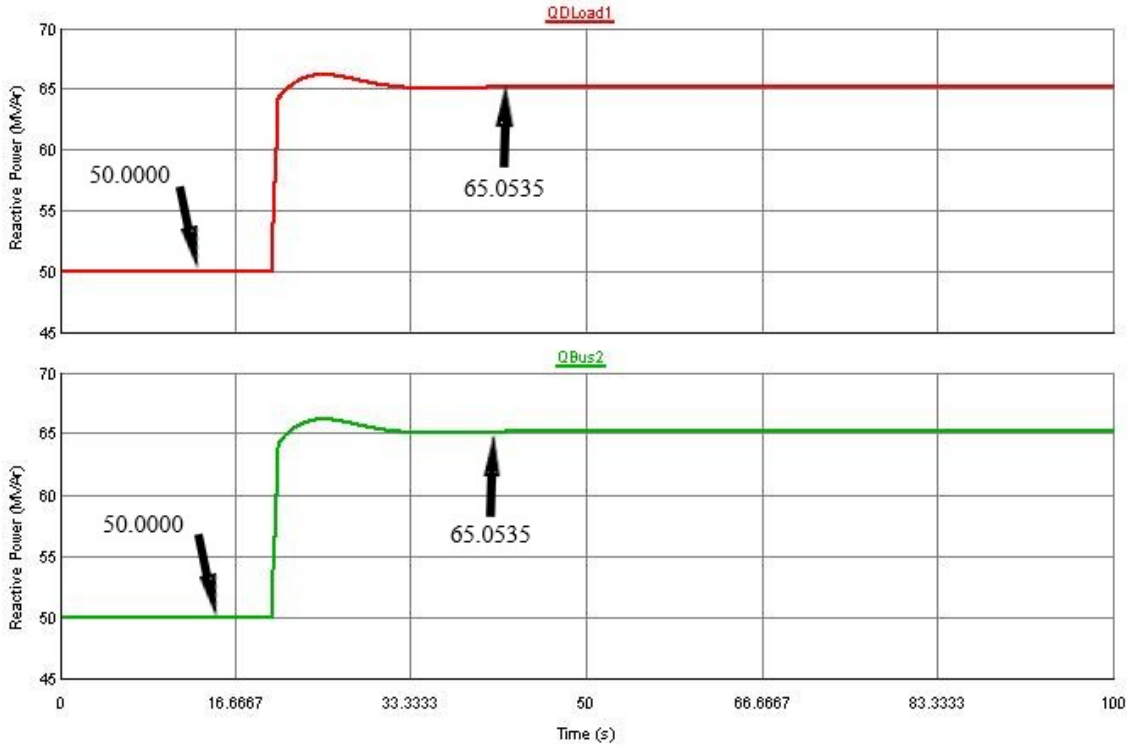


Figure 15. Increased load demand simulations for the power grid: Reactive power demand by DLoad1 and reactive power at Bus2.

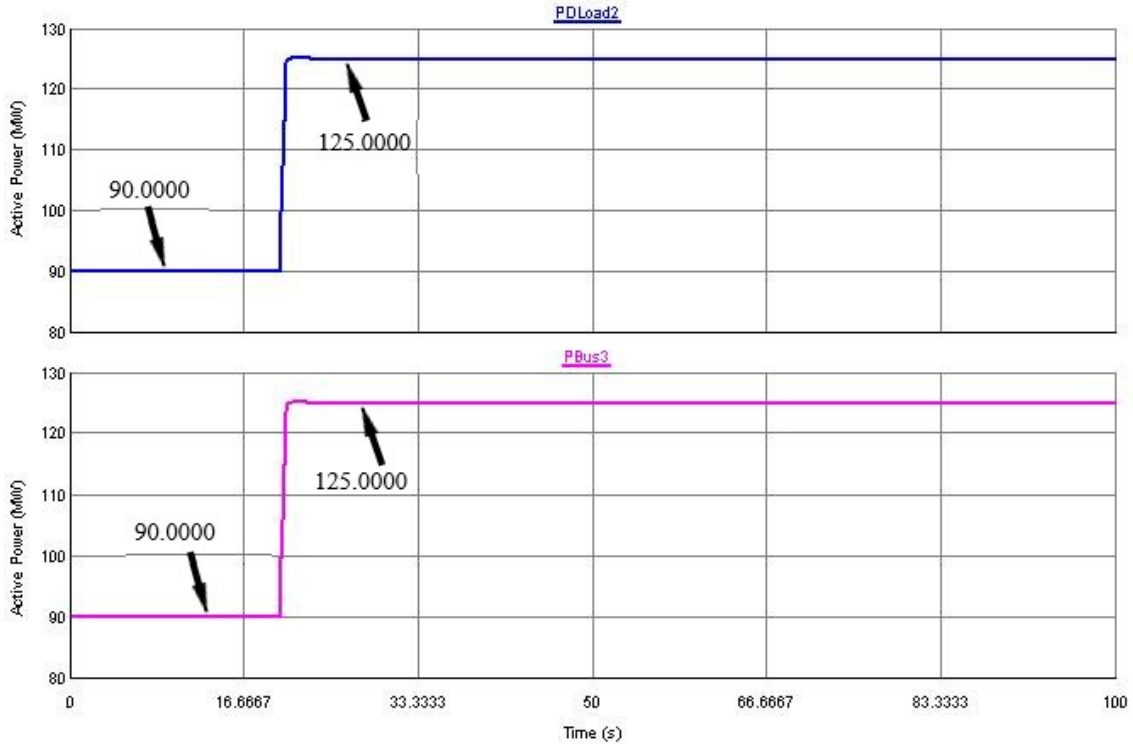


Figure 16. Increased load demand simulations for the power grid: Active power demand by DLoad2 and active power at Bus3.

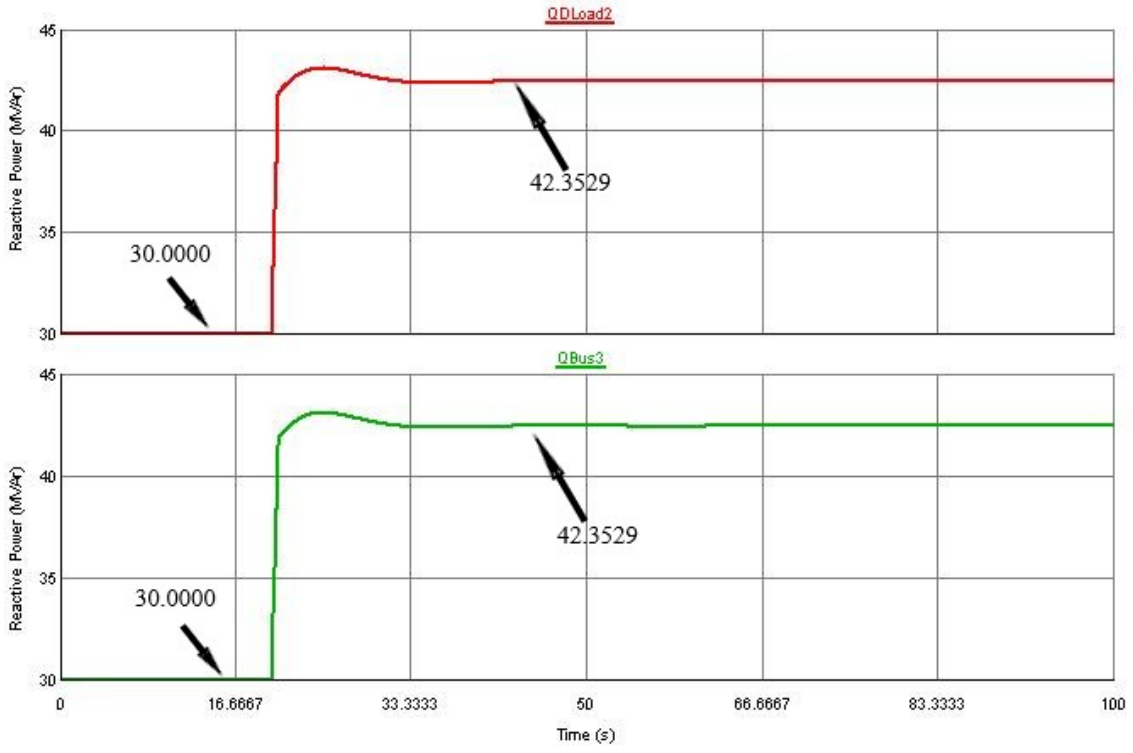


Figure 17. Increased load demand simulations for the power grid: Reactive power demand by DLoad2 and reactive power at Bus3.

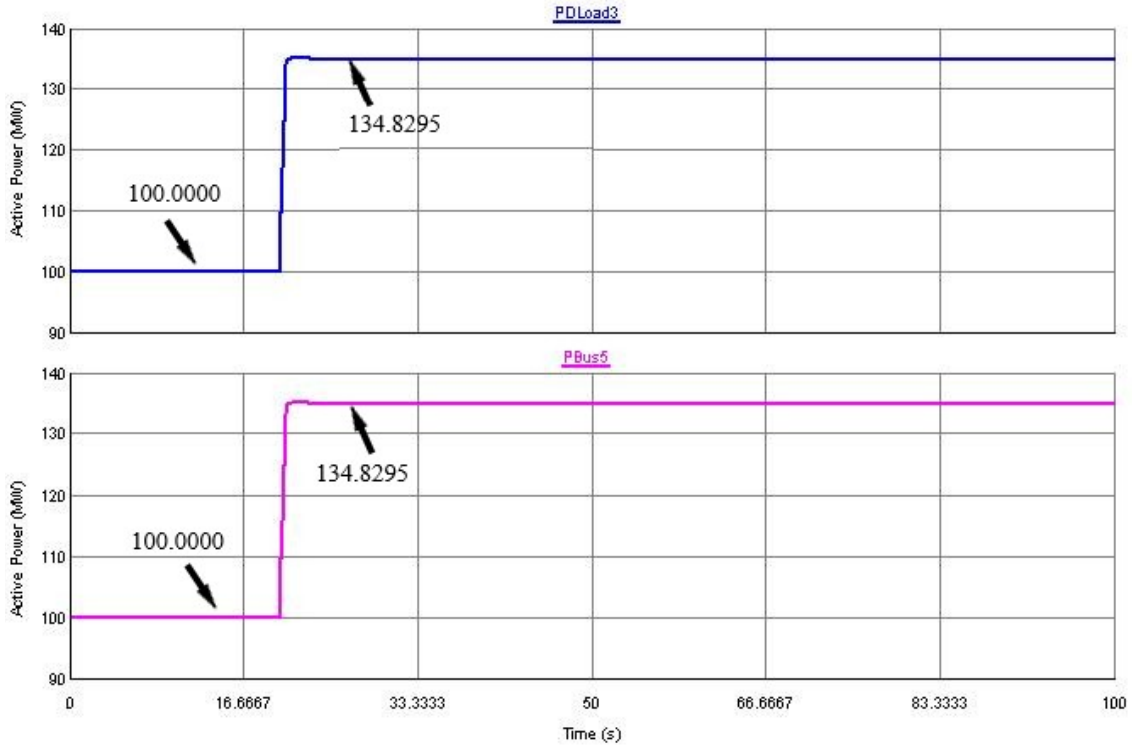


Figure 18. Increased load demand simulations for the power grid: Active power demand by DLoad3 and active power at Bus5.

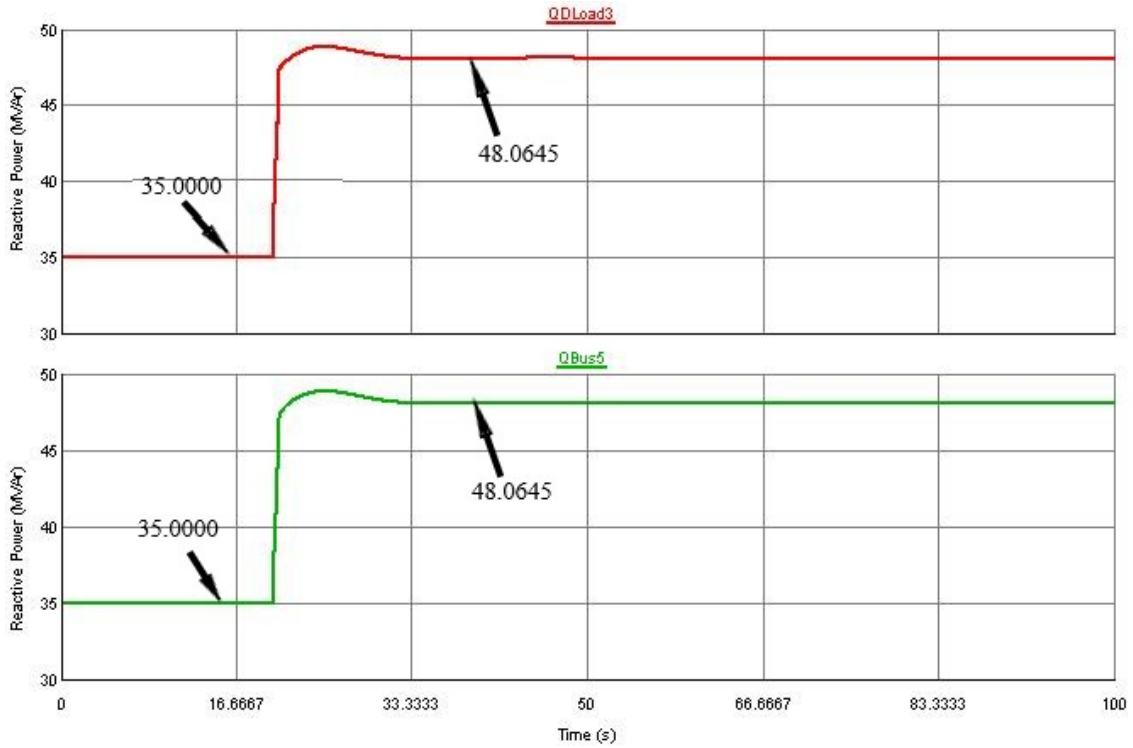


Figure 19. Increased load demand simulations for the power grid: Reactive power demand by DLoad3 and reactive power at Bus5.

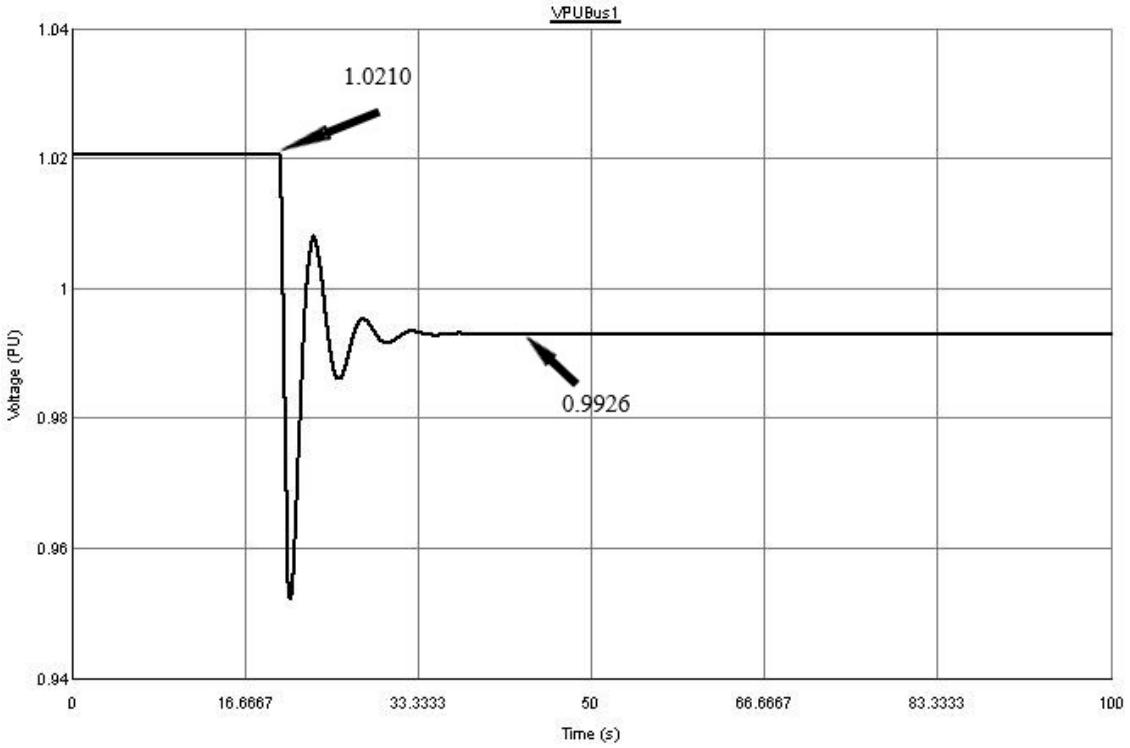


Figure 20. Increased load demand simulations for the power grid: Bus1 voltage.

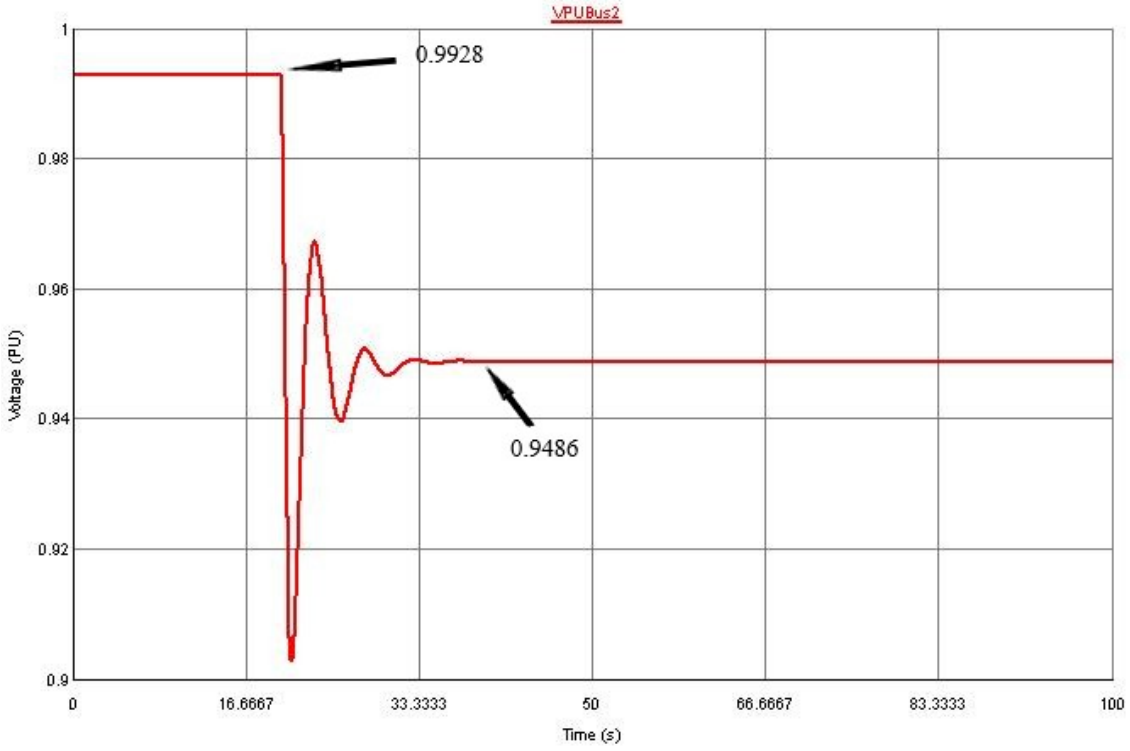


Figure 21. Increased load demand simulations for the power grid: Bus2 voltage.

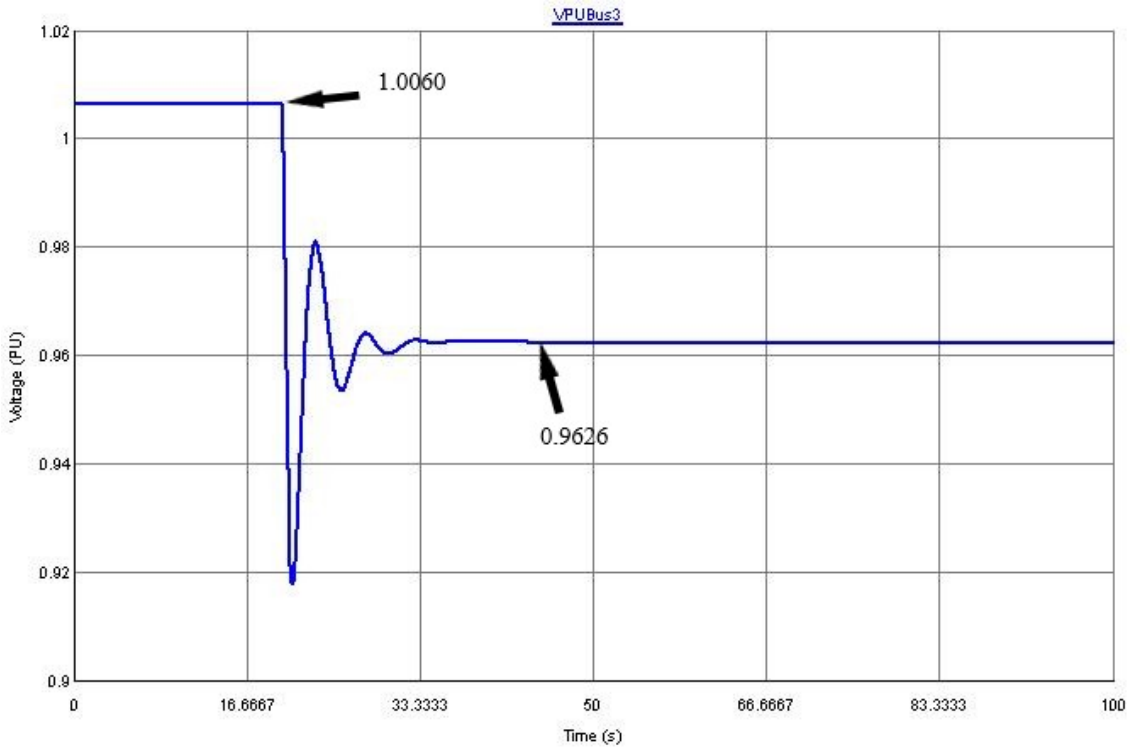


Figure 22. Increased load demand simulations for the power grid: Bus3 voltage.

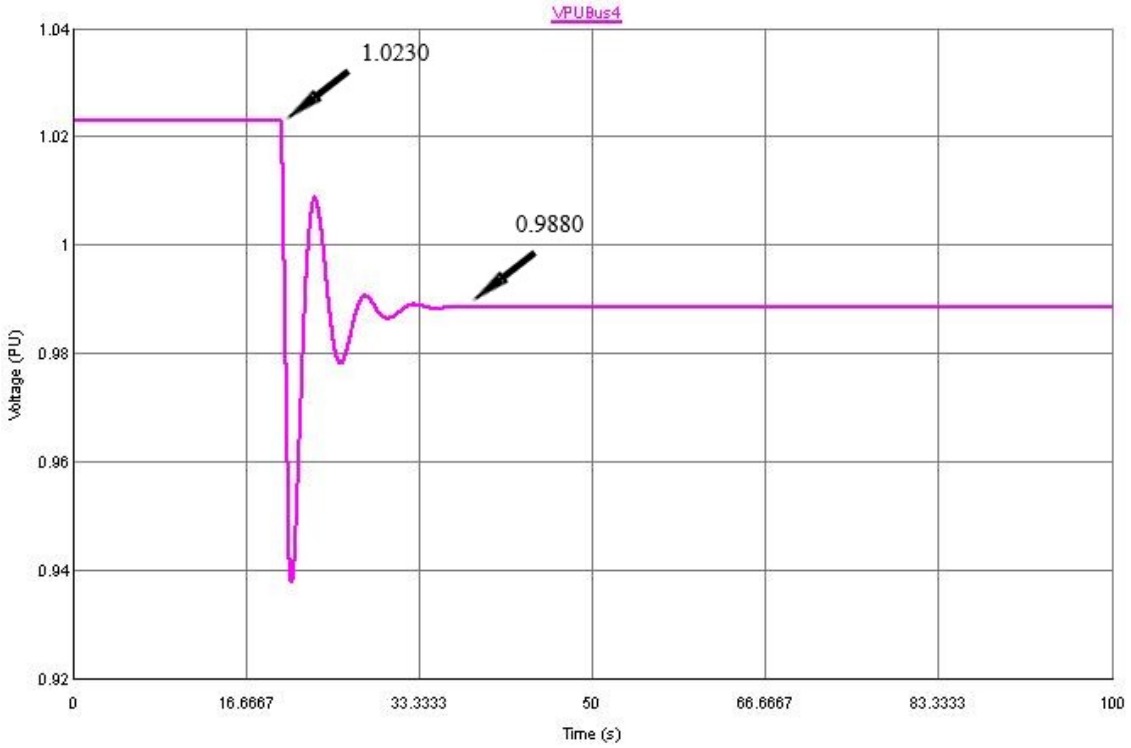


Figure 23. Increased load demand simulations for the power grid: Bus4 voltage.

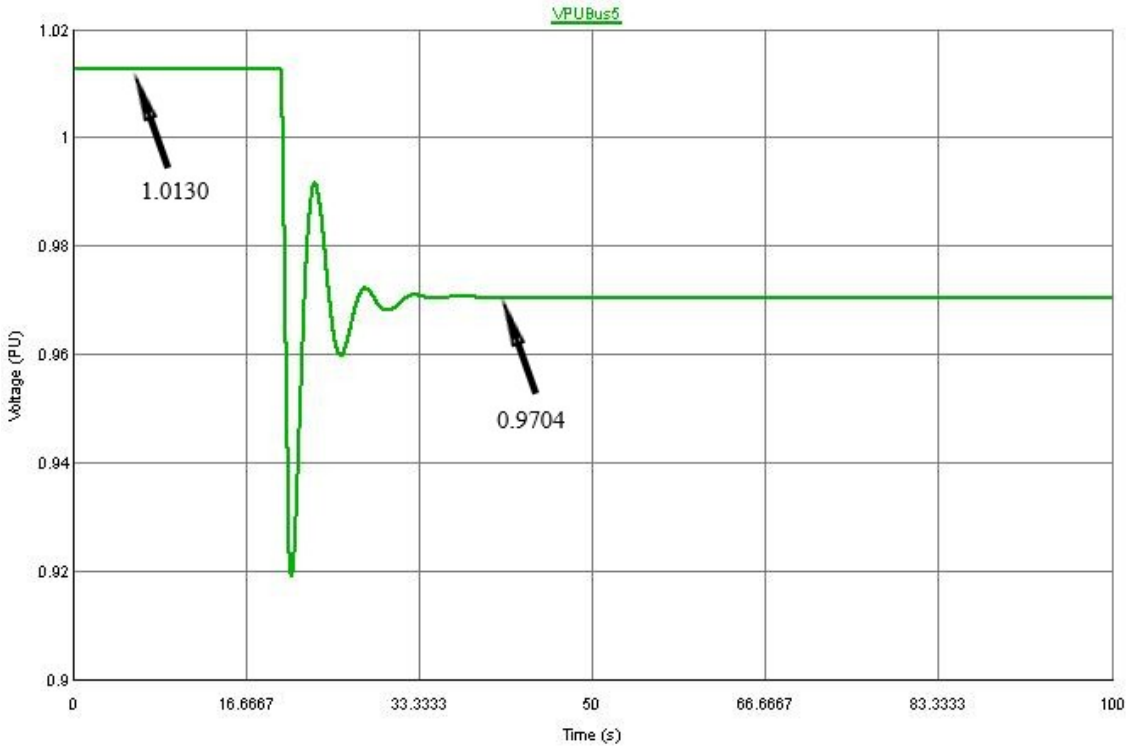


Figure 24. Increased load demand simulations for the power grid: Bus5 voltage.

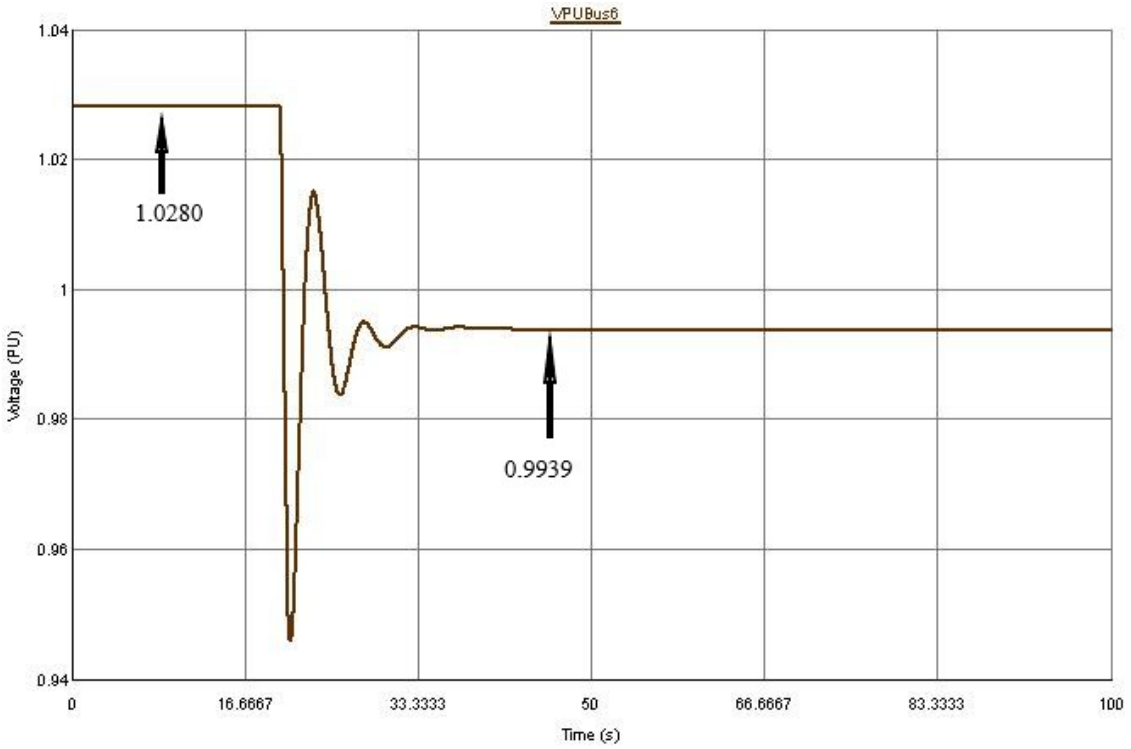


Figure 25. Increased load demand simulations for the power grid: Bus6 voltage.

In the simulation of the incremental load demand simulation performed above, we assessed the voltage stability thresholds and the compensation needed. This is how we studied the need to integrate the large-scale wind power plant (LSWPP) described below.

3.2. The Large-Scale Wind Power Plant Considered for the Study

The LSWPP used in this study is adapted from our previous study by the reference [36]. It consists of eighteen Type I upwind horizontal-axis wind turbine generator units (HAWTGUs) modeled from a combination of V117-4.2 MW and 4.0000 MW squirrel-cage induction generators (SCIGs) from Vestas' brochure and Appendix B Generator Parameters, respectively [37,38]. In total, the LSWPP has a capacity of 72.0000 MW. This capacity complements Category C WPP, which this document already refers to as the LSWPP.

Significantly, only simulation-related control components and other operating systems are described in this section so that the simulation of the system itself can be easily understood.

3.2.1. Preparation of the Large-Scale Wind Power Plant

The simulation of the LSWPP requires fundamental tuning of wind speed (m/s) and pitch angle adjustment (degrees). See Figure 26 for logic adapted from the same reference [36]. The control components shown in the figure are logically connected to the wind turbine (WT) model and are accessible for control on the RSCAD runtime module. In the same figure, *WT1PitchAngle* is the signal name to control the change in the pitch angle of the wind turbine, while *WindSpd1(km/h)* is the input wind speed to the wind turbine. The pitch angle is adjusted using a dial selector switch WT1PitchAngleAdjust with figures or positions 1 to 5. The wind speed is adjusted with a slider labeled WindSpd1Adjust. This logic is the same for all other WTs in the LSWPP model.

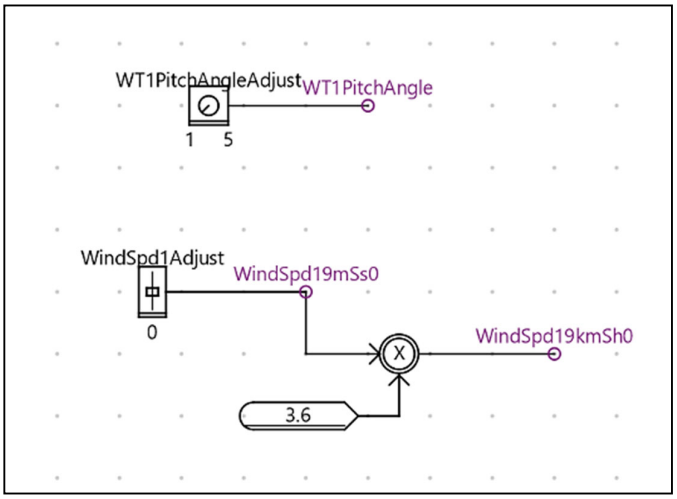


Figure 26. Logic for pitch angle and wind speed adjustments.

Other parameters like Default Air Temperature (DegC), Default Barometric Pressure (millibar), and Default Relative Humidity (%) do not need any additional control components to connect to them logically. Figure 27 shows the setting of these parameters on the WT model as viewed on the RSCAD draft module. By default, these parameters are accessible and can be tuned on the runtime module. Reference [36] can be visited for more information on how the LSWPP was modeled.

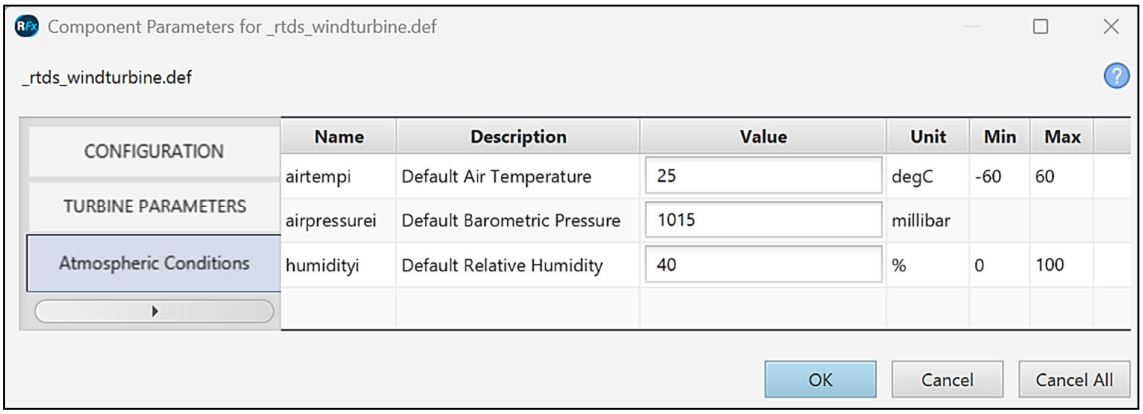


Figure 27. RSCAD draft wind turbine model parameters.

3.2.2. Large-Scale Wind Power Plant Simulations

The wind turbines (WTs) in the LSWPP model used in this study have operating temperatures between −20 °C and 45 °C. Nevertheless, WTs can be adjusted to generate the necessary output power almost equivalent to the rated output power as long as the temperature stays within the working range. Therefore, a temperature of 25 °C has been selected and used in this study.

The power coefficient, C_P, is also significantly influenced by air pressure and humidity. Humidity and air pressure were set to 30% and 1415 mbar, respectively, for the simulations. The sliders, dial selectors, and switches for these and other parameters in RSCAD runtime are shown in Figure 28.

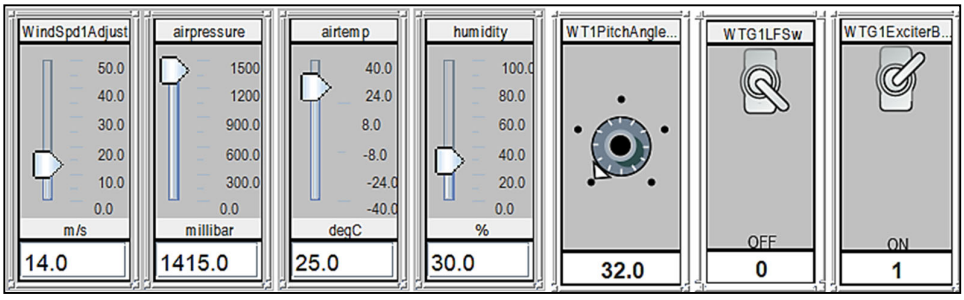


Figure 28. Sliders, dial selector switches, and control switches for a wind turbine. All other wind turbines in the model have the same setup of components for adjustments.

Simulations were performed for the LSWPP; the results are presented in Tables 12–14.

Table 12. Mechanical data for wind turbine generator units is monitored at steady-state power flow.

Quantities	Values
Wind speed	14.0000 m/s
Wind power	23.3100 MW
Wind turbine C_p	0.1720
Wind turbine power	4.0040 MW
Wind turbine rotor speed	9.9000 rpm
Wind turbine torque	3.8580 MN.m

Table 13. Wind turbine generator unit electrical data monitored at steady-state power flow.

Quantities	Values
WTGSU primary current	0.0160 kA
WTGSU secondary current	0.0010 kA
WTGU electrical torque	0.0100 PU
WTGU terminal voltage	1.0800 PU
WTGU exciter reactive power	2.1230 MVAr
WTGU active power (P) output	0.0240 MW
WTGU reactive power (Q) output	−2.0090 MVAr
WTGU reactive power circuit current	0.1600 kA

Table 14. Wind power plant sending-end data monitored at steady-state power flow.

Quantities	Values	
	Actual	Per Unit
Group 1 collector terminal voltage	26.0200 kV	1.0801 PU
Group 2 collector terminal voltage	26.0200 kV	1.0801 PU
Group 3 collector terminal voltage	26.0200 kV	1.0801 PU
WPP sending-end bus voltage	249.9000 kV	1.0801 PU
WPP receiving-end bus voltage	249.9000 kV	1.0801 PU
WPP sending-end frequency	50.0000 Hz	-
WPP receiving-end frequency	50.0000 Hz	-

3.2.3. Verifications of Renewable Energy Grid Code Specifications

The renewable energy grid codes (REGCs) specify the continuous operating per unit voltage level for Category C renewable power plants as 0.9000 (minimum) to 1.0985 (maximum). As shown in Table 14, under normal load flow conditions, the voltage measured on the high-voltage busbar of the modeled large-scale wind power plant (LSWPP) is at 1.0860 per unit, and is therefore acceptable. It is also stated that the RPP can run continuously at the frequency range between 49.0000 Hz and 51.0000 Hz. The frequency of the modeled LSWPP does not violate the continuous operating range specified by the grid codes, as it is at 50.0000 Hz under normal operating conditions. This means that the modeling and simulation (test) of the LSWPP model in this study were successful. This has also been attested in our previous study in reference [36].

4. Large-Scale Wind Power Plant Integration

Wind integration is the collection of all activities related to connecting the WPPs to the power grid. There are three high-level activities of grid integration, as listed in Table 15 [10].

Table 15. High-level activities of grid integration.

Planning	Physical Connection	System Operations
Power flow, short-circuit, and system stability studies	Build transmission from WPP to substation	Unit commitment
System operations study	Connection at substation	Economic dispatch
Wind power interconnection code	-	Wind energy forecasting

This study focused on planning, as it uses the simulation-based technique in proposing and (or) setting up a significant method of evaluating the operation of an interconnected system consisting of a LSWPP. Among the activities listed under planning, short-circuit studies are out of the current scope of this study.

The traditional electrical power grid and the LSWPP were studied individually in the previous sections. The LSWPP used has already been modeled with its transmission line for electrical power transmission to the busbar of selection (PCC) on the traditional power grid. Figure 29 illustrates the modern power grid formulated from the two systems studied above: the IEEE 9 Bus Power System and the LSWPP. The components WTGU1 to WTGU10 in the figure representing the first to the eighteenth wind turbine generator units. The LSWPP model and its components were modeled in subsystems (or racks) 3, 4, and 5. It was also shown in Section 3 that the IEEE 9 Bus Power System alone occupied subsystems 1 and 2.

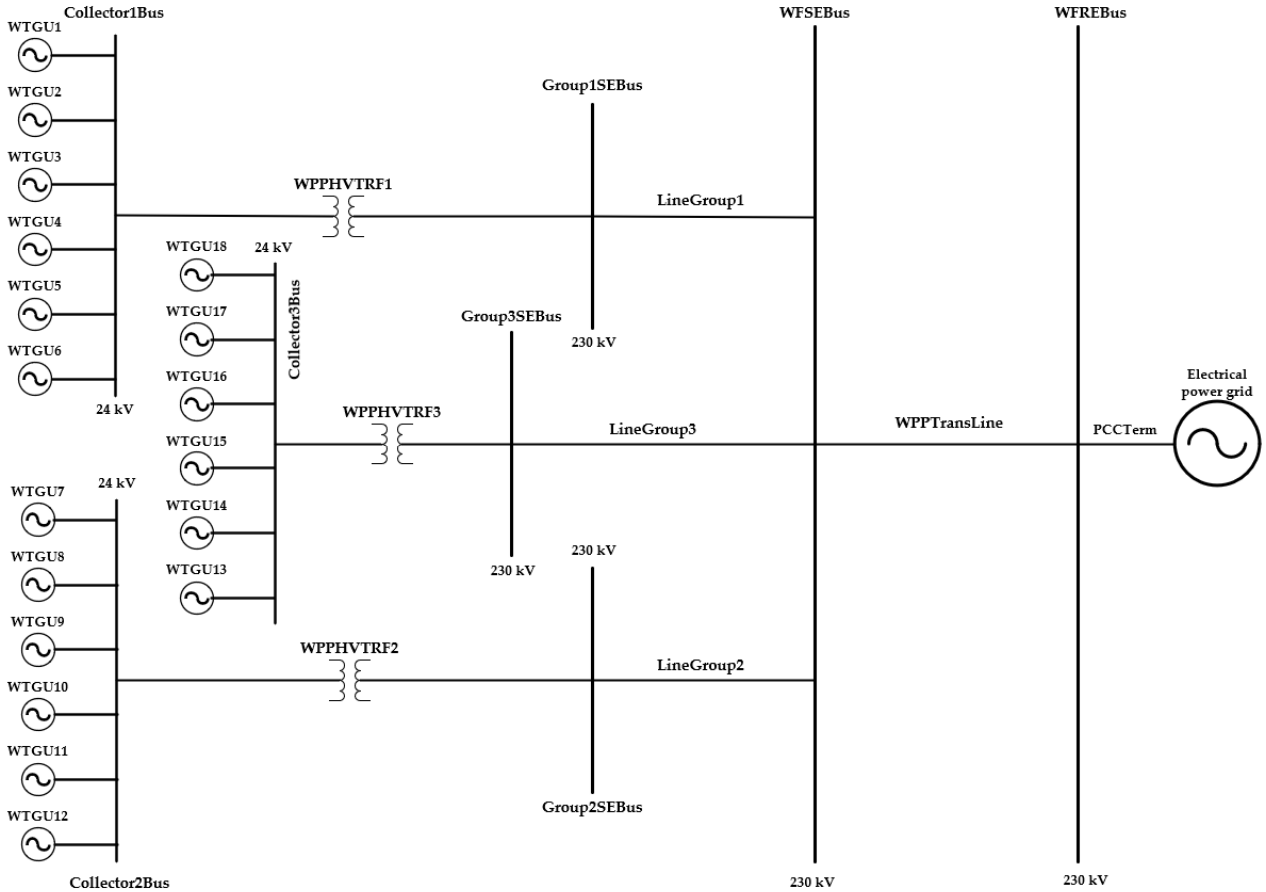


Figure 29. The resultant interconnected system (modern power grid) after coupling the LSWPP into Bus2 (PCC).

The WTGUs are a combination of wind turbines (WTs), squirrel-cage induction generators (SCIGs), and wind turbine generator substation unit transformers (WTGSUTs). It should be noted that the LSWPP used in this study consists of SCIGs whose output terminal voltage is 4 kV. These WTGSUTs step up to a medium voltage (MV) of 24 kV. This is to say that the voltage generated by each WTGU is considered MV and is distributed through the LSWPP MV circuit. This is the voltage where the high-voltage (HV) step-up power transformers (WPPHVTRFs) step up for transmission over the lines LineGroup1, LineGroup2, and LineGroup3, and then over the transmission line, WPPTransLine, to the grid point of connection (PCC). PCCTerm in the figure is the point of common coupling

(PCC) terminal. It connects the LSWPP to the electrical power grid through Bus2, which was discussed in the early sections.

The parameters of the modern power grid (interconnected system) are listed in Appendix B of this article.

After integration, there is an additional transmission line circuit interconnecting the LSWPP, which, according to the renewable energy grid codes (REGCs), depending on the agreement between the power system operator (PSO) and the WPP operator (WPPO), this transmission line can either be operated by the PSO or the WPPO. At this point, attention was only given to monitoring from the sending-end busbar (WFSEBus) and receiving-end busbar (WFSEBus) up to the traditional electrical power grid side.

5. Evaluation of the Grid-Connected Mode of Operation of a Large-Scale Wind Power Plant

Case studies were executed to determine if the electrical quantities in the interconnected system were according to the renewable energy grid codes (REGCs). The case studies first looked at the initial load simulations to check if the busbar voltages were within the acceptable values. After that, the increased load demand was simulated to check if the voltages at the busbars had improved and were settling at acceptable values based on the power grid operating standards.

5.1. Initial Load Demand Simulations for the Modern Power Grid System

In this simulation, we put the load demand at its initial stage and monitored the load and busbar active and reactive power, as tabulated in Tables 16 and 17. We also recorded busbar voltage values, as shown in Table 18.

Table 16. Active power on load busbars and their loads under initial load demand for the modern power grid.

	Load Active Power (MW)	Busbar Active Power (MW)
DLoad1 | Bus2	125.0000	125.0000
DLoad2 | Bus3	90.0000	90.0000
DLoad3 | Bua5	100.0000	100.0000

Table 17. Reactive power on load busbars and their loads under initial load demand for the modern power grid.

	Load Reactive Power (MVAr)	Busbar Reactive Power (MVAr)
DLoad1 | Bus2	50.0000	50.0000
DLoad2 | Bus3	30.0000	30.0000
DLoad3 | Bua5	35.0000	35.0000

Table 18. Busbar voltage under initial load demand for the modern power grid.

Busbars	Voltage (PU)
Bus1	1.0210
Bus2	0.9928
Bus3	1.0060
Bus4	1.0230

Table 18. *Cont.*

Busbars	Voltage (PU)
Bus5	1.0130
Bus6	1.0280
WPPSEBus	0.9930
WPPREBus	0.9934

5.2. Increased Load Demand Simulations for the Modern Power Grid System

Our analysis in this section is based on Bus2 only since it has already been identified as the critical busbar in previous sections. While the attention was focused on Bus2, the load demand increase simulation was again performed, and the active power and reactive power for both DLoad1 and Bus2, along with voltage results pertinent to this busbar, have been recorded in Figures 30, 31, and 32, respectively.

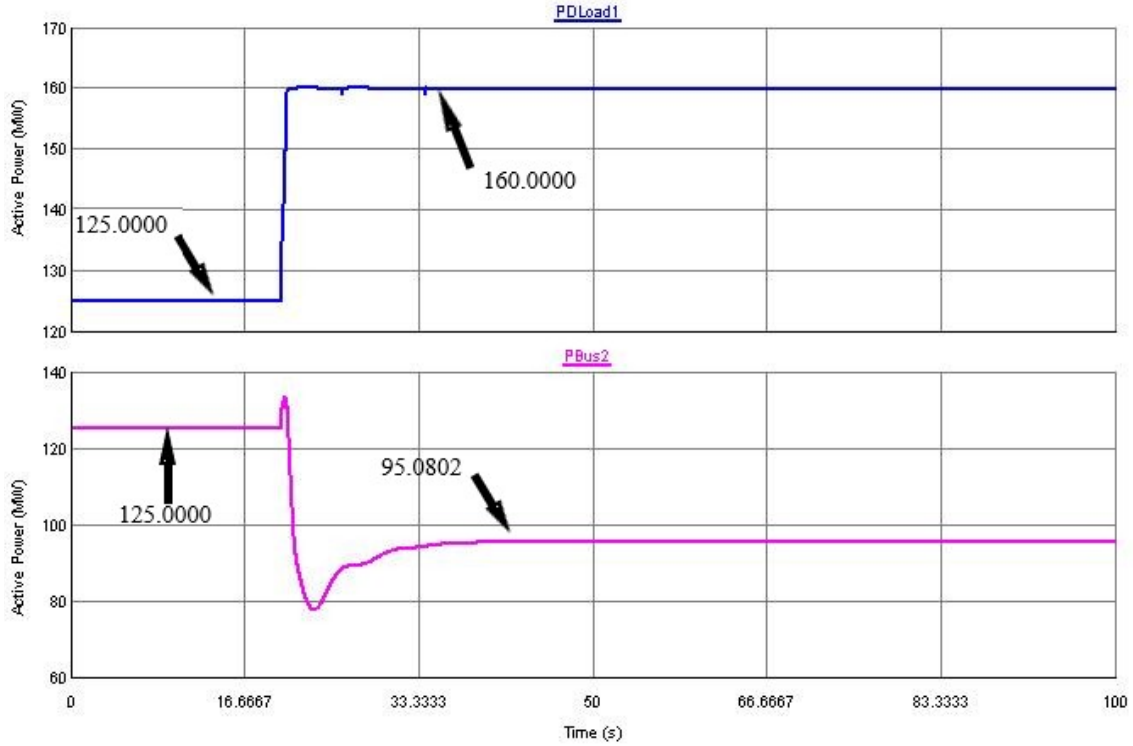


Figure 30. Increased load demand simulations for the modern power grid: Active power demand by DLoad1 and active power at Bus2.

The voltage Bus2 was again observed during this simulation in response to the load demand increase in DLoad1. With an increase in load demand, the voltage at Bus2 dropped less significantly compared to the standalone traditional power grid.

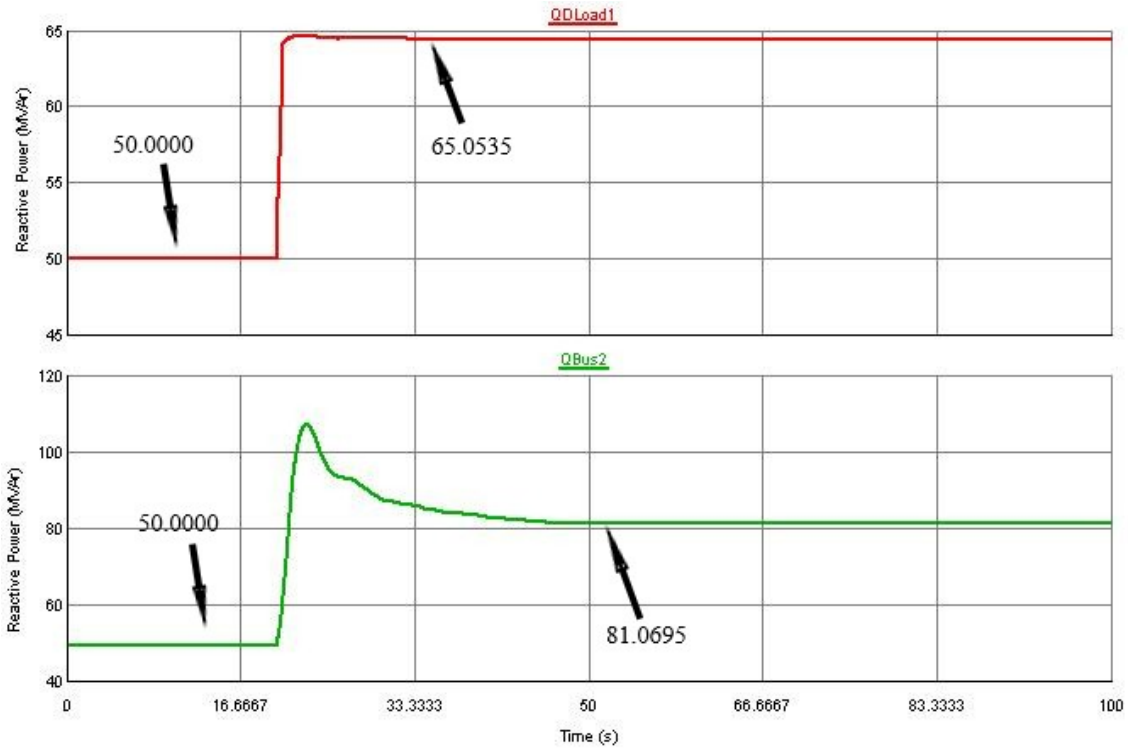


Figure 31. Increased load demand simulations for the modern power grid: Reactive power demand by DLoad1 and reactive power at Bus2.

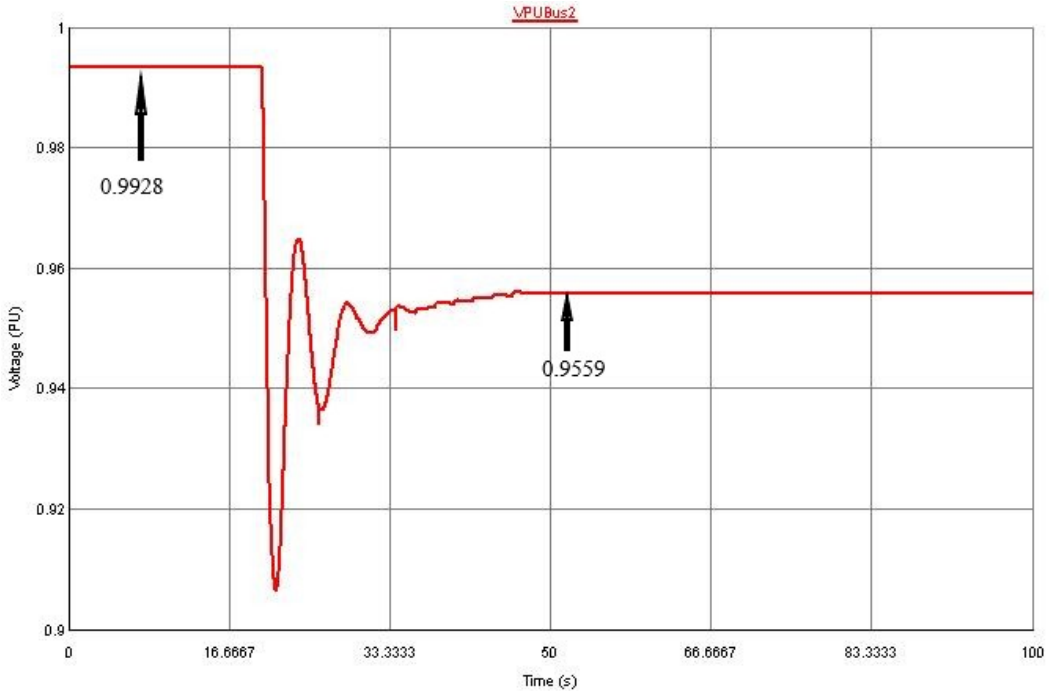


Figure 32. Increased load demand simulations for the modern power grid: Bus2 voltage.

6. Discussion of Results

When the load demand increase was implemented, a significant improvement in the voltage stability of the electrical power grid system was revealed after integrating the large-scale wind power plant (LSWPP) into this study. This finding is not new. However, the approach to reaching it is new in the following manner. The existing studies, like [19–21] rarely consider a step-by-step approach to obtaining to this finding. They did not consider

evaluating the renewable energy grid code specifications before integrating the developed systems into the electrical power grid. Unlike the existing studies, this study aligned with the design and operational requirements of WPPs mentioned in [22–24]. This is due to its approach of first considering the simulations of the developed LSWPP alone to ensure its operation meets the REGC specifications before integrating it into the considered power grid. Furthermore, some studies on wind power plant (WPP) integration use a reasonable megawatt capacity of a single WTGU and treat it as a LSWPP, for instance, in reference [17]. Considering the models used in [17], and other models in [18–21], the computation time was saved. The challenge is that the models developed in these studies may not provide adequate validation to align the REGCs, whose significance has been mentioned in the work published in the references [1,3,4,14,26] for LSWPPs in the grid-connected mode of operation.

Lastly, using the Real-Time Digital Simulator (RTDS) devices with their software Real-time Simulation Computer-Aided Design (RSCAD) in this study enabled the simulation of load disturbance while monitoring them in real time. This has made the overall simulations in the study realistic compared to other studies.

7. Conclusions and Future Work

This work evaluated the large-scale wind power plant (LSWPP) grid-connected mode of operation by considering grid code specifications in real-time simulation. The studies associated with this topic have been explored. The interconnected system consisting of a LSWPP considered in this study has been carefully selected and, most importantly, described. Case studies have been conducted in consideration of the specifications of renewable energy grid codes (REGCs). The interconnected system developed and considered in this study effectively evaluates the grid-connected mode of operation of an LSWPP. It can be used for other large-scale renewable power plant (LSRPP) systems like photovoltaic (PV) systems.

It should be noted that in a WPP, not all wind turbine generator units (WTGUs) are operated simultaneously. This study considered the worst-case scenario where all WTGUs were required to operate simultaneously when the contribution of the entire WPP was urgently required. This is the part we will need to improve on when studying the need for WPP integration in the future, and we also look at developing a controller to ensure that the supply power required from the WPP side does not approach to the rated capacity.

Before this work, we had our previous work listed as follows:

(1) We first looked at the design of wind power plants (WPPs) and modeled a large-scale wind power (LSWPP) in [36].
(2) We performed a recap on the existing control methods for modern power grids consisting of WPPs.
(3) We evaluated the power grid voltage instability point using system overloading contingency in real-time simulation.
(4) Following the work in (3), we recently tested the busbar differential protection system, based on practical considerations, using a real-time digital simulator hardware-in-the-loop (HIL) testing technique.

Future work will consider a cross-comparison case study, applying the model developed in this study to a different international grid code to demonstrate its adaptability and robustness.

Author Contributions: Conceptualization, S.N., M.E.S.M. and A.K.R.; methodology, S.N., M.E.S.M. and A.K.R.; software, S.N., M.E.S.M. and A.K.R.; validation, S.N., M.E.S.M. and A.K.R.; formal analysis, S.N., M.E.S.M. and A.K.R.; investigation, S.N., M.E.S.M. and A.K.R.; resources, S.N., M.E.S.M. and A.K.R.; data curation, S.N., M.E.S.M. and A.K.R.; writing—original draft preparation, S.N., M.E.S.M. and A.K.R.; writing—review and editing, S.N., M.E.S.M. and A.K.R.; visualization, S.N., M.E.S.M. and A.K.R.; supervision, S.N., M.E.S.M. and A.K.R.; project administration, S.N., M.E.S.M. and A.K.R.; funding acquisition, S.N., M.E.S.M. and A.K.R. All authors have read and agreed to the published version of the manuscript.

Funding: This research received no external funding.

Institutional Review Board Statement: Not applicable.

Informed Consent Statement: Not applicable.

Data Availability Statement: The original contributions presented in this study are included in the article. Further inquiries can be directed to the corresponding author.

Acknowledgments: We thank the Center for Substation Automation and Energy Management Systems (CSAEMS). This research would not have been possible without their facilities.

Conflicts of Interest: The authors declare no conflict of interest.

Abbreviations

The following abbreviations are used in this manuscript.

WT	Wind turbine
WTGU	Wind turbine generator unit
WTGSUT	Wind turbine generator substation unit transformer
WFSEBus/WPPSEBus	Wind farm/wind power plant sending-end busbar
WPPHVTRF	Wind power plant high-voltage transformer
WFREBus/WPPREBus	Wind farm/wind power plant receiving-end busbar
G1Bus, G2Bus, and G3Bus	Generator 1 busbar, Generator 2 busbar, and Generator 3 busbar
G1, G2, and G3	Generator 1, Generator 2, and Generator 3
DLoad1, DLoad2, and DLoad3	Dynamic load 1, Dynamic load2, and Dynamic load 3
Bus1, Bus2, Bus3, Bus4, Bus5, and Bus6	Busbar 1, Busbar 2, Busbar 3, Busbar 4, Busbar 5, and Busbar 6
RSCAD	Real-time Simulation Computer-Aided Design
RTDS	Real-Time Digital Simulator
HIL	Hardware-In-the-Loop
WPP	Wind power plant
LSWPP	Large-scale wind power plant
REGC	Renewable energy grid code
RPP	Renewable power plant
PU	Per unit
WPPTransLine	Wind power plant transmission line
PCCTerm	Point of common coupling terminal
SEBus	Sending-end busbar
REBus	Receiving-end busbar

Appendix A

This section presents a flowchart of the overall study, as shown in Figure A1.

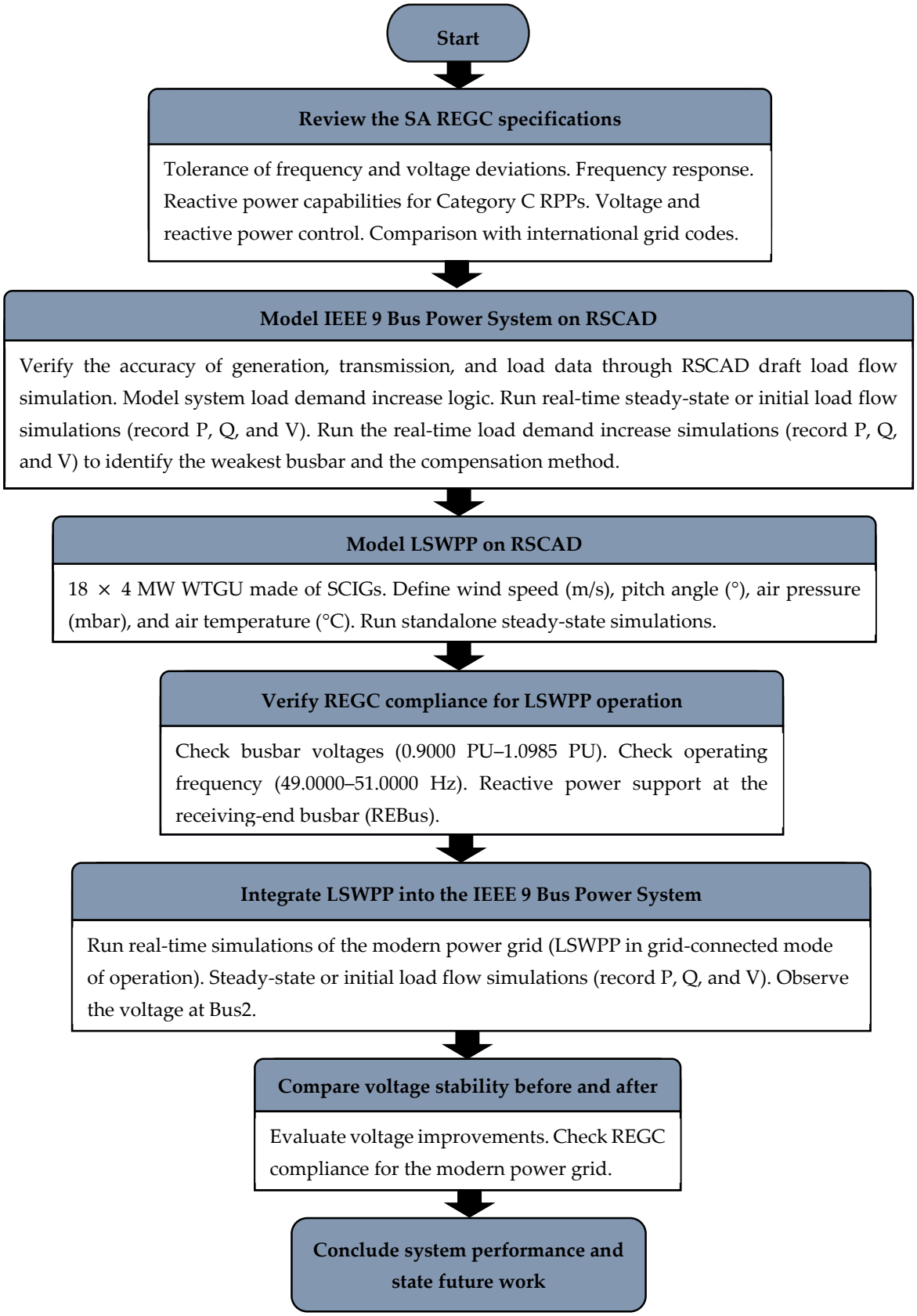


Figure A1. A flowchart showing all steps that were followed to conduct the study.

Appendix B

This section shows other parameters for the IEEE 9 Bus Power System combined with those of the large-scale wind power plant (LSWPP). All per unit values have been derived from a base apparent power of 100 MVA.

Table A1. Large-scale wind power plant transmission line parameters.

Lines	The Busbar to Which Line Is Connected	Length (km)	Resistance (PU)	Reactance (PU)	Susceptance (PU)
LineGroup1	Group1SEBus—WF1SEBus	15.0000	-	-	-
LineGroup2	Group2SEBus—WF1SEBus	15.0000	-	-	-
LineGroup3	Group3SEBus—WF1SEBus	15.0000	-	-	-
WPPTransLine					

All other wind turbine generator unit (WTGU) group lines, LineGroup2 and LineGroup3, are the same as the ones shown in Figure A2.

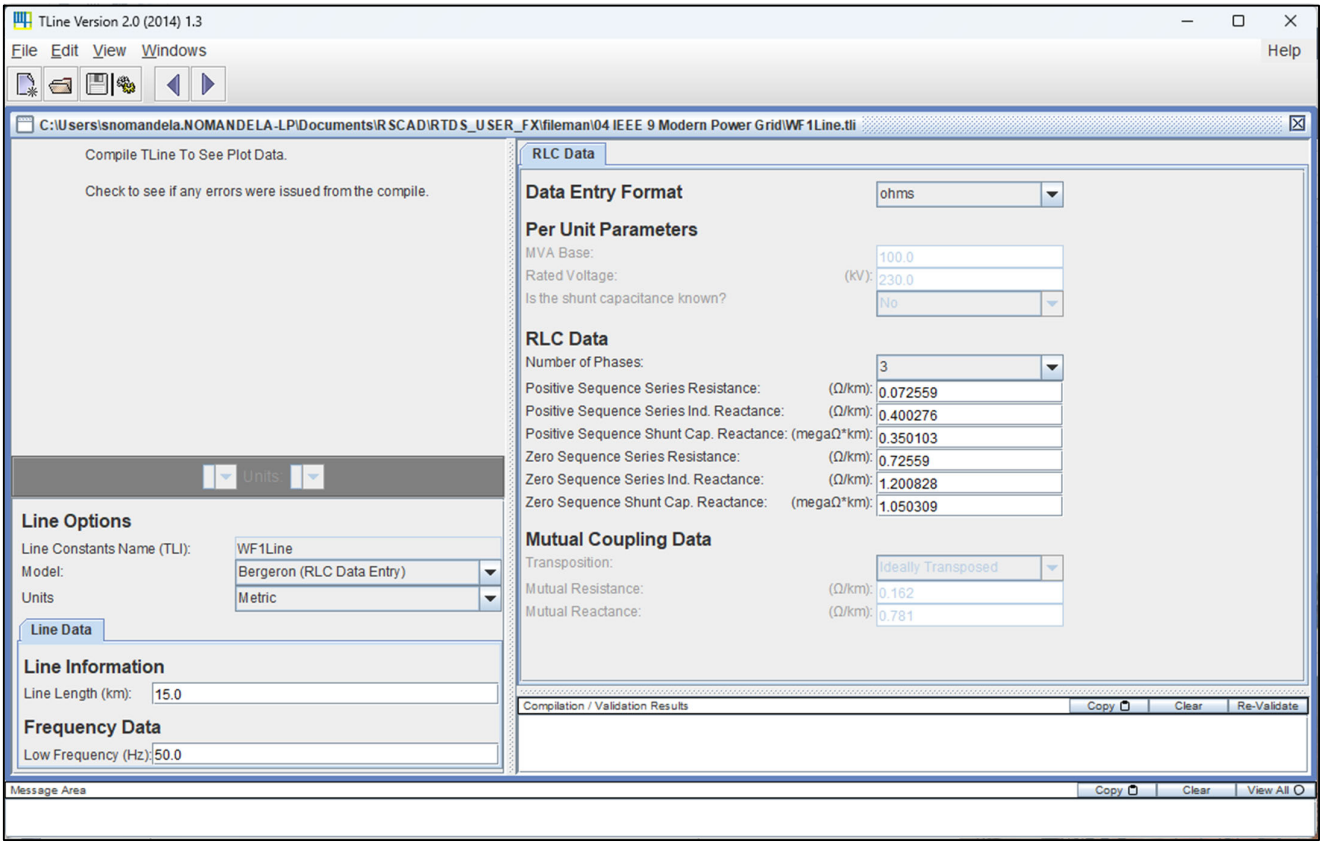


Figure A2. LSWPP LineGroup1 transmission line parameters.

Table A2. Power transformer parameters.

Transformer	The Busbar to Which the Power Transformer Is Connected	Voltage Rating (kV)	Resistance (PU)	Inductive Reactance (PU)	Capacity (MVA)
TRF1	G1Bus–Bus1	16.5/230	0.0	0.0576	100
TRF2	G2Bus–Bus4	18/230	0.0	0.0625	100
TRF3	G3Bus–Bus6	13.8/230	0.0	0.0586	100
WTGU1Trans	WTG1Terminal–Collector1Bus	4/24	-	-	5
Group1Trans	Collector1Bus–Group1Bus	24/230	-	-	30

The parameters for the transformer WTGU1Trans are the same as those of the WTGU2Trans and WTGU2Trans up to WTGU18Trans for other WTGUs. The other WTGU groups, Group2Trans and Group3Trans, are the same as Group1Trans. The IEEE 9 Bus Power System consists of three generators with their controllers, governors and exciter controllers. Tables A3 and A4 show the generator parameters.

Table A3. IEEE 9 Bus Power System generator parameters 1.

Generator	The Busbar to Which the Generator Is Connected	Xa (PU)	Xd (PU)	Xd′ (PU)	Xd″ (PU)	Xq (PU)	Xq′ (PU)	Xq″ (PU)
Gen1	G1Bus	0.0146	0.1460	0.0608	0.0600	0.1000	0.0969	0.0600
Gen2	G2Bus	0.0896	0.8958	0.1198	0.1100	0.8645	0.1969	0.1100
Gen3	G3Bus	0.1313	1.3125	0.1813	0.1800	1.2578	0.2500	0.1800

Table A4. IEEE 9 Bus Power System generator parameters 2.

Generator	The Busbar to Which the Generator Is Connected	Ra (PU)	Tdo′ (s)	Tdo″ (s)	Tqo′ (s)	Tqo″ (s)	H (s)	D (PU/PU)
Gen1	G1Bus	0.00013	8.9600	0.0100	0.3100	0.0100	23.6400	0.0
Gen2	G2Bus	0.00013	6.0000	0.0100	0.5350	0.0100	6.4000	0.0
Gen3	G3Bus	0.00013	5.8900	0.0100	0.6000	0.0100	3.0100	0.0

Table A5. Vestas V117-4.2 MW wind turbine and rotor data.

Parameter	Values
Rotor diameter (D_R)	117 m
Swept area (A_S)	10.7510 m^2
Minimum turbine angular speed, ω_{TRMin}	2.1000 rpm = 0.2200 rad/s
Nominal turbine angular speed, ω_{TRN}	9.9000 rpm = 1.0350 rad/s
Maximum turbine angular speed, ω_{TRMax}	17.7000 rpm = 1.8500 rad/s

Table A6. Vestas V117-4.2 MW wind turbine operating data [36].

Parameter	Values
Nominal power (P_N)	4.0000 MW/4.2000 MW
Cut-in-speed (v_{CI})	3.0000 m/s
Nominal speed (v_N)	14.0000 m/s
Cut-out-speed (v_{CO})	25.0000 m/s
Re-cut-in-speed (V_{R-CI})	23.0000 m/s
Wind class	EC IB-T/IEC IIA-T/IEC S-T
Standard operating temperatures	−20 °C to 45 °C with de-rating above 30 °C at 4 MW
Nominal power (P_N)	4.0000 MW/4.2000 MW
Cut-in-speed (v_{CI})	3.0000 m/s
Nominal speed (v_N)	14.0000 m/s

Table A7. Squirrel-cage induction generator parameters [36].

Parameter	Actual Values	Per Unit (PU) Values
Rated output power	4.0000 MW	-
Rated mechanical power	4.0606 MW	
Rated apparent power	4.8420 MVA	
Rated line-to-line voltage	40,000 V (rms)	
Rated phase voltage = Base voltage	2309.4000 V (rms)	
Rated stator current = Base current	698.8800 A (rms)	
Rated stator frequency	50.0000 Hz	
Rated power factor	0.8261	
Rated rotor speed	1510.5000 rpm	
Rated mechanical torque	25.6710 kN.m	
Rated stator flux linkage	7.3917 Wb (rms)	
Rated rotor flux linkage	6.7114 Wb (rms)	
Stator winding resistance	22.1040 mΩ	0.0067
Rotor winding resistance	23.1515 mΩ	0.0069
Stator leakage inductance	1.6980 mH	
Stator leakage reactance	j0.53344 Ω	j0.1615
Rotor leakage inductance	1.6980 mH	
Rotor leakage reactance	j0.53344 Ω	j0.1615
Magnetizing inductance	33.5970 mH	
Magnetizing reactance	j10.5548 Ω	j3.1946
Base flux linkage	7.3511 Wb (rms)	
Base impedance	3.3044 Ω	
Base inductance	10.5180 mH	
Base capacitance	963.2900 μF	

The letter j represents the reactance values of the machine.

References

1. Ahmed, S.D.; Al-Ismail, F.S.M.; Shafiullah, M.; Al-Sulaiman, F.A.; El-Amin, I.M. Grid Integration Challenges of Wind Energy: A Review. *IEEE Access* **2020**, *8*, 10857–10878. [CrossRef]
2. Osman, A.M.; Alsokhiry, F. Sliding Mode Control for Grid Integration of Wind Power System Based on Direct Drive PMSG. *IEEE Access* **2022**, *10*, 26567–26579. [CrossRef]
3. Ibrahim, H.; Ghandour, M.; Dimitrova, M.; Ilinca, A.; Perron, J. Integration of Wind Energy into Electricity Systems: Technical Challenges and Actual Solutions. *Energy Procedia* **2011**, *6*, 815–824. [CrossRef]
4. Yuan, X. Overview of Problems in Large-scale Wind Integrations. *J. Mod. Power Syst. Clean Energy* **2013**, *1*, 22–25. [CrossRef]
5. Abdelghany, M.B.; Mariani, V.; Liuzza, D.; Natale, O.R.; Glielmo, L. A Unified Control Platform and Architecture for the Integration of Wind-Hydrogen Systems into the Grid. *IEEE Trans. Autom. Sci. Eng.* **2023**, *21*, 4042–4057. [CrossRef]
6. Wu, D.; Seo, G.-S.; Xu, L.; Su, C.; Kocewiak, L.; Sun, Y.; Qin, Z. Grid Integration of Offshore Wind Power: Standards, Control, Power Quality and Transmission. *IEEE Open J. Power Electron.* **2024**, *5*, 583–604. [CrossRef]

7. Pandit, D.; Bera, A.; Saket, R.K. Probabilistic Sizing of Energy Storage Systems for Reliability and Frequency Security in Wind-Rich Power Grids. *IEEE Access* **2024**, *12*, 4608–4621. [CrossRef]
8. Li, L.; He, J.; Niu, J.; Liu, H.; Yu, X.; Huang, Y.; Zhang, X. A Phase-to-Phase Protection Algorithm With the Transient Information for the Wind Power Plant Transmission Line. *IEEE Access* **2024**, *12*, 100581–100590. [CrossRef]
9. Rekik, M.; Abdelkafi, A.; Krichen, L. Synchronization of wind farm power system to utility grid under voltage and frequency variations. *Int. J. Renew. Energy Res.* **2015**, *5*, 70–81.
10. Jain, P.; Wijayatunga, P. Grid Integration of Wind Power: Best Practices for Emerging Wind Markets. *Sustain. Dev. Work. Pap. Ser.* **2016**. Available online: https://www.adb.org/publications/grid-integration-wind-power-best-practices-wind-markets (accessed on 17 March 2025).
11. Tummala, A.; Velamati, R.K.; Sinha, D.K.; Indraja, V.; Krishna, V.H. A Review on Small Scale Wind Turbines. *Renew. Sustain. Energy Rev.* **2016**, *56*, 1351–1371. [CrossRef]
12. Masters, G.M. *Renewable and Efficient Electric Power Systems*; Wiley and Sons, Inc: Hoboken, NJ, USA, 2004. [CrossRef]
13. Stock, A.; Amos, L.; Alves, R.; Leithead, W. Design and Implementation of a Wind Farm Controller using Aerodynamics Estimated from LIDAR Scans of Wind Turbine Blades. In Proceedings of the 2021 American Control Conference (ACC), New Orleans, LA, USA, 25–28 May 2021; pp. 1790–1795. [CrossRef]
14. Blazquez, F.; Veganzones, C.; Martinez, S. Large Scale Integration of Wind Energy into Power Systems. *Electr. Power Qual. Utilis. Mag.* **2005**, *1*, 15–22.
15. Abbas, S.R.; Kazmi, S.A.A.; Naqvi, M.; Javed, A.; Naqvi, S.R.; Ullah, K.; Khan, T.-U.; Shin, D.R. Impact Analysis of Large-Scale Wind Farms Integration in Weak Transmission Grid from Technical Perspectives. *Energies* **2020**, *13*, 5513. [CrossRef]
16. Xu, D.; Mu, G.; Liu, H.; Yan, G. Assessment on Large-scale Offshore Wind Farm Integration. In Proceedings of the 2014 9th IEEE Conference on Industrial Electronics and Applications (ICIEA 2014), Hangzhou, China, 9–11 June 2014; IEEE: New York, NY, USA, 2014; pp. 556–559. [CrossRef]
17. Rana, V.; Gupta, R.; Kumar, N. Integration of Wind Farm into A Weak Distribution Network. *Change* **2014**, *4*, 404–409.
18. Hasnaoui, O.; Allagui, M. Dynamic performance improvement of wind farms equipped with three SCIG generators using STATCOM. *J. Energy South. Afr.* **2014**, *25*, 128–135. [CrossRef]
19. Benseddik, A.; Kouba, N.; Boudour, M.; Hasni, M.; Menaa, M. Wind Farm Integration Intermittency Impact on Power System Transient Stability. In Proceedings of the 2018 International Conference on Electrical Sciences and Technologies in Maghreb (CISTEM), Algiers, Algeria, 28–31 October 2018; pp. 1–6. [CrossRef]
20. Xia, S.; Zhang, Q.; Hussain, S.T.; Hong, B.; Zou, W. Impacts of Integration of Wind Farms on Power System Transient Stability. *Appl. Sci.* **2018**, *8*, 1289. [CrossRef]
21. Rachdi, T.; Saoudi, Y.; Mahmoud, I.; Florin, I.; Errachdi, A. The Impact of Integration Wind Turbine on the Stability of the Electricity Grid. In Proceedings of the 2022 IEEE Information Technologies & Smart Industrial Systems (ITSIS), Mankato, MN, USA, 19–21 May 2022; pp. 1–6. [CrossRef]
22. Niwas, S.; Singh, S.N.; Ostergaard, J.; Jain, N. Distributed Generation in Power Systems: An Overview and Key Issues. In Proceedings of the 24th Indian Engineering Congress (IEC), Kyoto, Japan, 10–13 December 2009. Available online: https://backend.orbit.dtu.dk/ws/portalfiles/portal/5202512/24IEC_paper.pdf (accessed on 17 March 2025).
23. Sewchurran, S.; Davidson, I.E. Introduction to the South African Renewable Energy Grid Code version 2.9 requirements (Part II—Grid code technical requirements). In Proceedings of the 2017 IEEE AFRICON, Cape Town, South Africa, 18–20 September 2017; pp. 1225–1230. [CrossRef]
24. National Energy Regulator of South Africa. Grid Connection Code for Renewable Power Plants Connected to the Electricity Transmission System or the Distribution System in South Africa. Vol. 1, No. January. National Energy Regulator of South Africa, Germiston, pp. 1–113. 2022. Available online: https://www.nersa.org.za/wp-content/uploads/bsk-pdf-manager/2022/01/SAGC-Requirements-for-Renewable-Power-Plants-Rev-3.1.pdf (accessed on 17 March 2025).
25. Nomandela, S.; Ratshitanga, M.; Mnguni, M.E.S. IEC 61850 Standard-Based Protection of the Coupling Point Between a Wind Farm and the Power Grid. Cape Peninsula University of Technology (CPUT). 2021. Available online: https://www.researchgate.net/publication/370501543_IEC_61850_Standard-based_Protection_of_the_Coupling_Point_Between_a_Wind_Farm_and_the_Power_Grid (accessed on 17 March 2025).
26. Meiqi, Y.; Liangzhong, Y. Integration of Large Scale Wind Farm into Electrical Grids. In Proceedings of the 2010 China International Conference on Electricity Distribution (CICED2010), Nanjing, China, 13–16 September 2010; IEEE: New York, NY, USA, 2010; pp. 1–5.
27. ESKOM. *Transmission and Distribution of Electricity, No. Revision 11*; ESKOM: Sandton, South Africa, 2021; pp. 1–3.
28. Davidson, I.E. Introduction to the South African Renewable Energy Grid Code Version 2.9 Requirements. In Proceedings of the 2017 IEEE AFRICON, Cape Town, South Africa, 18–20 September 2017; pp. 1263–1267. [CrossRef]
29. Plc, N.G.E.T. The Grid Code—UK, No. 5. 2017. Available online: https://www.neso.energy/document/85301/download (accessed on 17 March 2025).

30. Hooper, J.W.; Chester, R.O. *Technical Guidelines for Power Generating Units and Systems. Certification of the Electrical Characteristics of Power Generating Units and Systems in Medium-, High and Extra-High Voltage Grids*; Fördergesellschaft Windenergie und Andere Erneuerbare Energien: Berlin, Germany, 2016; pp. 51–136. [CrossRef]
31. *IEEE Std 1547-2018 (Revision of IEEE Std 1547-2003)*; IEEE Standard for Interconnection and Interoperability of Distributed Energy Resources with Associated Electric Power Systems Interfaces. IEEE: New York, NY, USA, 2016.
32. RTDS Technologies. *IEEE 9 Bus Power System*; RTDS Technologies: Winnipeg, MB, Canada, 2019; pp. 2–5.
33. Marison, G.; Gao, B.; Kundur, P. Voltage Stability Analysis Using Static and Dynamic Approaches. *IEEE Trans. Power Electron.* **1993**, *8*, 1159–1171. [CrossRef]
34. Kundur, P.; Paserba, J.; Ajjarapu, V.; Andersson, G.; Bose, A.; Canizares, C.; Hatziargyriou, N.; Hill, D.; Stankovic, A.; Taylor, C.; et al. Definition and Classification of Power System Stability. *IEEE Trans. Power Syst.* **2004**, *19*, 3271–3281. [CrossRef]
35. Kundur, P. *Power System Stability and Control*; McGraw: New York, NY, USA, 1993.
36. Nomandela, S.; Mnguni, M.E.S.; Raji, A.K. Modeling and Simulation of a Large-Scale Wind Power Plant Considering Grid Code Requirements. *Energies* **2023**, *16*, 2897. [CrossRef]
37. Vestas. 4 MW Wind Platform. Brocher. 2017. Available online: https://www.vestas.com/en/products/4-mw-platform (accessed on 17 March 2025).
38. Wu, B.; Lang, Y.; Zargari, N.; Kouro, S. Power Conversion and Control of Wind Energy Systems: Appendix B: Generator Parameters. In *Wind Energy*; John Wiley & Sons: Hoboken, NJ, USA, 2011; pp. 319–326.

Disclaimer/Publisher's Note: The statements, opinions and data contained in all publications are solely those of the individual author(s) and contributor(s) and not of MDPI and/or the editor(s). MDPI and/or the editor(s) disclaim responsibility for any injury to people or property resulting from any ideas, methods, instructions or products referred to in the content.